

Manuscript Number: EPSL-D-18-00847R1

Title: Pronounced northward shift of the westerlies during MIS 17 leading to the strong 100-kyr ice age cycles

Article Type: Letters

Keywords: Mid-Pleistocene Transition, southwestern Europe, pollen, vegetation, precipitation, temperature

Corresponding Author: Professor maria fernanda sanchez goni,

Corresponding Author's Institution:

First Author: maria fernanda sanchez goni

Order of Authors: maria fernanda sanchez goni; Patrizia Ferretti, Dr; Josué M Polanco-Martinez, Dr; Teresa Rodrigues, Dr; Montserrat Alonso-Garcia, Dr; Francisco Javier Rodriguez-Tovar, Dr; Javier Dorador, Dr; Stéphanie Desprat, Dr

Abstract: The MIS 17 interglacial, ~715 - 675 ka, marks the end of the Mid-Pleistocene Transition as intensified, long and asymmetrical 100-kyr ice age cycles became eminently established. Increasing arrival of moisture to the Northern Hemisphere high latitudes, resulting from the northwestward migration of the Subpolar Front and the intensification of the Norwegian Greenland Seas (NGS) convection, has been put forward to explain the emergence of this quasi-periodic 100-kyr cycle. However, testing this hypothesis is problematic with the available North Atlantic precipitation data. Here we present new pollen-based quantitative seasonal climate reconstructions from the southwestern Iberian margin that track changes in the position and intensity of the westerlies. Our data compared to changes in North Atlantic deep and surface water conditions show that MIS 17 interglacial was marked by three major changes in the direction and strength of the westerlies tightly linked to oceanographic changes. In particular, we report here for the first time a drastic two-steps northward shift of the westerlies centered at ~ 693 ka that ended up with the sustained precipitation over southern European. This atmospheric reorganization was associated with northwestward migration of the Subpolar Front, strengthening of the NGS deep water formation and cooling of the western North Atlantic region. This finding points to the substantial arrival of moisture to the Northern Hemisphere high latitudes at the time of the decrease in summer energy and insolation contributing to the establishment of strong 100-kyr cycles.

Significant statement (116 words, maximum 120 words)

- Strongest expansion of the Mediterranean forest of the last 800,000 years
- Maximum summer warmth in SW Iberia during the peak of the cool MIS 17
- Pronounced two-step northward shift of the westerlies centered at ~693 ka
- Increasing arrival of moisture at northern high latitudes at the end of MIS 17
- Important contribution of the westerlies in explaining the strong 100-kyr ice cycles

1 **Pronounced northward shift of the westerlies during MIS 17 leading to the strong 100-kyr**
2 **ice age cycles**

3

4 María Fernanda Sánchez Goñi^{a,b,*}, Patrizia Ferretti^c, Josué M. Polanco-Martínez^{b,d}, Teresa
5 Rodrigues^{e,f}, Montserrat Alonso-García^{e,f}, Francisco Javier Rodríguez-Tovar^g, Javier Dorador^h,
6 Stéphanie Desprat^{a,b}

7

8 ^aEcole Pratique des Hautes Etudes (EPHE, PSL University), F-33615 Pessac, France

9 ^bUniversity of Bordeaux, EPOC, UMR 5805, F-33615 Pessac, France

10 ^cConsiglio Nazionale delle Ricerche, Istituto per la Dinamica dei Processi Ambientali (CNR-
11 IDPA), Venice I-30123, Italy

12 ^dBasque Centre for Climate Change – BC3, Sede Building 1, 1st floor Scientific Campus of the
13 University of the Basque Country, 48940 Leioa, Spain

14 ^eDivisão de Geologia e Georecursos Marinhos, Instituto Português do Mar e da Atmosfera,
15 Rua Alfredo Magalhães Ramalho, 6, 1495-006 Lisboa, Portugal

16 ^fCentro de Ciências do Mar (CCMAR), Universidade do Algarve, Campus de Gambelas, 8005-
17 139 Faro, Portugal

18 ^gDepartamento de Estratigrafía y Paleontología, Universidad de Granada, Avda. Fuentenueva
19 s/n, 18002 Granada, Spain

20 ^hDepartment of Earth Sciences, Royal Holloway University of London, Egham, Surrey TW20
21 OEX, UK

22

23 * Corresponding author: María Fernanda Sánchez Goñi

24 Ecole Pratique des Hautes Etudes (EPHE, PSL University), UMR EPOC, University of
25 Bordeaux, Allée Geoffroy St Hilaire 33615, Pessac, France

26 Phone: +33 5 40 00 83 84

27 e-mail: maria.sanchez-goni@u-bordeaux.fr

28

29

30

31 **Abstract**

32 The MIS 17 interglacial, ~715 - 675 ka, marks the end of the Mid-Pleistocene
33 Transition as intensified, long and asymmetrical 100-kyr ice age cycles became eminently
34 established. Increasing arrival of moisture to the Northern Hemisphere high latitudes,
35 resulting from the northwestward migration of the Subpolar Front and the intensification of
36 the Norwegian Greenland Seas (NGS) convection, has been put forward to explain the
37 emergence of this quasi-periodic 100-kyr cycle. However, testing this hypothesis is
38 problematic with the available North Atlantic precipitation data. Here we present new
39 pollen-based quantitative seasonal climate reconstructions from the southwestern Iberian
40 margin that track changes in the position and intensity of the westerlies. Our data compared
41 to changes in North Atlantic deep and surface water conditions show that MIS 17 interglacial
42 was marked by three major changes in the direction and strength of the westerlies tightly
43 linked to oceanographic changes. In particular, we report here for the first time a drastic
44 two-steps northward shift of the westerlies centered at ~ 693 ka that ended up with the
45 sustained precipitation over southern European. This atmospheric reorganization was
46 associated with northwestward migration of the Subpolar Front, strengthening of the NGS
47 deep water formation and cooling of the western North Atlantic region. This finding points
48 to the substantial arrival of moisture to the Northern Hemisphere high latitudes at the time
49 of the decrease in summer energy and insolation contributing to the establishment of strong
50 100-kyr cycles.

51

52

53 **Keywords:** Mid-Pleistocene Transition, southwestern Europe, pollen, vegetation,

54 precipitation, temperature

55 **1. Introduction**

56 The Marine Isotopic Stage (MIS) 17 interglacial, ~715,000-675,000 years ago (715-675
57 ka), preceded the onset of the firmly established 100-kyr ice age cycles at ~650 ka (MIS 16)
58 (Bahr et al., 2018; Elderfield et al., 2012; Hodell and Channell, 2016; Mudelsee and
59 Stattegger, 1997; Wright and Flower, 2002) . Both, proxy data (Ehlers and Gibbard, 2007;
60 Hodell et al., 2008; Naafs et al., 2013) and model simulations (Bintanja and van de Wal,
61 2008) suggest that the North American ice sheets surpassed the Eurasian ice masses to
62 become the dominant ice accumulations of the Northern Hemisphere. This switch to greater
63 ice accumulation in North America coincided with a major reorganization of both surface
64 and deep North Atlantic oceanic currents when the “Boreal heat pump” was replaced by the
65 “Nordic heat pump” implying a northwest migration of the Subpolar Front (Alonso-Garcia et
66 al., 2011; Imbrie et al., 1993; Wright and Flower, 2002) and the intensification of the North
67 Atlantic deep water formation (Poirier and Billups, 2014). This hypothesis assigns a key role
68 to the “Nordic heat pump” in establishing the strong 100-kyr cyclicity of the late Pleistocene
69 glacial cycles because it enhanced the moisture transport to the northern high latitudes that
70 promoted ice sheets build-up. Likewise, deep water formation mainly occurred in the
71 Subpolar North Atlantic before 700 ka causing reduced poleward heat transport (Imbrie et
72 al., 1993; Wright and Flower, 2002). Well-established 100-kyr cycles would therefore have
73 been started by a change between a long period of advection of warm water that enhanced
74 moisture transport to southern Europe and the growth of Alpine glaciers (Bahr et al., 2018)
75 and a period of a decreasing trend in the sea surface temperature (SST) east-west gradient
76 (Alonso-Garcia et al., 2011; Wright and Flower, 2002) associated with the northward shift of
77 the westerlies that brought warmth and precipitations to northern Europe. However, no
78 data exists so far demonstrating the sustained arrival of high amounts of moisture to

79 southern Europe during MIS 17 and the subsequent northward shift of precipitation to
80 colder regions of the Northern Hemisphere feeding the ice caps.

81 Here we present the first record of atmospherically-driven vegetation dynamics in
82 southwestern Europe during the MIS 17 interglacial testing if the reconfiguration of oceanic
83 and atmospheric circulation during MIS 17 might have preconditioned enhanced ice sheet
84 growth during MIS 16. We analyzed the pollen preserved in the southwestern Iberian margin
85 IODP site U1385 (Fig. 1) to infer regional vegetation changes and quantitatively reconstruct
86 seasonal and annual temperatures and precipitation. The westerlies are responsible for most
87 of the precipitation arriving in Europe (Brayshaw et al., 2010) and the main factor currently
88 controlling vegetation greenness, an indicator of forest cover, in the Iberian Peninsula
89 (Gouveia et al., 2008). This direct relationship between westerlies and forest cover in Iberia
90 makes pollen-inferred forest cover changes recorded in the U1385 sedimentary record be
91 ideally suited to track past shifts in the position of the westerlies. We performed numerical
92 zonation and time series analyses (change point method and Fourier and wavelet spectral
93 analysis) on the Mediterranean forest pollen record to identify significant changes in the
94 vegetation and therefore in the westerlies, and the dominant cyclicities. Changes in the type
95 and rate of sedimentation based on ichnofabric analysis provide additional information on
96 major shifts in local deep water conditions. Our vegetation-based westerlies record was then
97 compared with changes in $\delta^{18}\text{O}$ of benthic foraminifera ($\delta^{18}\text{O}_b$) (Hodell and Channell, 2016;
98 Hodell et al., 2015) and sea surface conditions from the same site (Bahr et al., 2018; Martin-
99 Garcia et al., 2015; Rodrigues et al., 2017), and with other North Atlantic records of surface
100 and deep ocean changes documented further north and west (Alonso-Garcia et al., 2011;
101 Naafs et al., 2013; Poirier and Billups, 2014; Wright and Flower, 2002) (Fig. 1).

102

103 **2. Present-day environmental setting**

104 IODP Site U1385 (37°34.285'N, 10°7.562'W, 2578 m depth) is located on a spur, the
105 Promontorio dos Principes de Avis. The sedimentary section recovered at Site U1385 (1.5
106 km-long record) shows hemipelagic continental margin sediments deposited under normal
107 marine conditions with a fully oxygenated water column and average sedimentation rates of
108 10 cm/ky (Stow et al., 2013). The surface water column at the site is affected by the Portugal
109 current (PC) which brings cold nutrient-rich water from the northern latitudes and forms the
110 Eastern North Atlantic Central Waters of subpolar origin (ENACWsp), and by the Azores
111 current (AC) which brings warm water from the Azores front generating the ENACW of
112 subtropical origin (ENACWst) (Ríos et al., 1992). ENACWsp underlies the ENACWst and form
113 the permanent thermocline down to c. 500 m water depth (Fig. 1).

114 The present-day climate of southwestern Iberia, 1961-1990 period, is Mediterranean with
115 warm and dry summers and mild and wet winters. During winter the North Atlantic
116 westerlies bring moisture to the Iberian margin (Fig. 1), while a high pressure cell develops in
117 the North Atlantic during summer, which generates strong northerly trade winds inducing
118 coastal upwelling (Fiúza et al., 1982). The mean winter (DJF) and summer (JJA) precipitation
119 is 250 and less than 50 mm, respectively (80 and <20 mm/month) (Miranda et al., 2002);
120 mean winter and summer temperatures are at around 10°C and 22°C, respectively (Ramos et
121 al., 2011). This strong seasonality lead to the development of a Mediterranean vegetation in
122 the adjacent landmasses dominated by deciduous oak at middle elevation (700-1000 m
123 a.s.l.), and evergreen oak, olive tree, *Pistacia*, *Phillyrea* and rockroses (*Cistus*) at lower
124 elevations (Blanco Castro et al., 1997).

125

126 **3. Material and Methods**

127 3.1 Stratigraphy and age model

128 The stratigraphy of Site U1385 was built upon a combination of chemo-stratigraphic
129 proxies (Hodell et al., 2015). Ca/Ti ratio measured every cm in all holes by core scanning XRF
130 was used to construct a composite section, and low resolution (20 cm) oxygen isotopes of
131 benthic foraminifera ($\delta^{18}\text{O}_b$). For consistency with previous works from the same site
132 (Sánchez Goñi et al., 2016), the age model of the studied interval was based, among the two
133 age models proposed by Hodell et al. (2015), on the correlation of the $\delta^{18}\text{O}_b$ record to the
134 marine $\delta^{18}\text{O}_b$ stack of LR04 (Lisiecki and Raymo, 2005) (Table S1).

135

136 3.2 Pollen analysis and quantitative climatic reconstruction

137 Sediment subsamples 1-cm thick and 2.5-4 cm³ volume were prepared for pollen
138 analysis using an optimized protocol for marine samples, [http://www.ephe-](http://www.ephe-paleoclimat.com/Files/Other/Pollen%20extraction%20protocol.pdf)
139 [paleoclimat.com/Files/Other/Pollen%20extraction%20protocol.pdf](http://www.ephe-paleoclimat.com/Files/Other/Pollen%20extraction%20protocol.pdf), employing coarse-
140 sieving at 150 μm , successive treatments with cold HCl, cold HF at increasing concentration
141 and micro-sieving (10 μm mesh). At the beginning of the treatment, we added known
142 quantities of *Lycopodium* spores in tablet form to calculate pollen concentration. Slides were
143 prepared using a mobile mounting medium, i.e. glycerol, to permit rotation of the pollen
144 grains and a transmitted Primo Star light microscope was used for routine identification of
145 pollen and spores at 400 \times and 1000 \times magnifications. One hundred samples were analyzed
146 every 4 cm in average. Excluding ten samples with pollen counts between 50 and 100, pollen
147 counts oscillate between 100 and 166 terrestrial pollen grains excluding *Pinus*, aquatics and
148 spores (total sporo-pollen sum between 117 and 754). The number of pollen morphotypes in
149 most of the samples, 78 samples out from 100, ranges from 20 to 27, and from 13 to 19
150 morphotypes in the remaining samples. Pollen percentages for terrestrial taxa were

151 calculated against the main sum of terrestrial grains, while percentages for *Pinus* were
152 calculated against the main sum plus *Pinus*. Aquatic pollen and spores percentages are based
153 on the total sum (Pollen + spores + indeterminables + unknowns). We assume that the
154 average uncertainty of the calculated pollen percentage values in our analysis is less than
155 8%, based on the average error of 7.9% calculated by (Fletcher and Sanchez Goñi, 2008).
156 Total sporo-pollen concentrations oscillate between 9000 and 147,000 grains.cm⁻³ (Fig. S1).
157 Changes in grain concentrations do not parallel changes in pollen percentages and,
158 therefore, these latter changes indicate actual variations in forest cover and composition.
159 However, one should keep in mind that the relationship between arboreal pollen
160 percentages and forest cover is not direct, which is mostly due to the difficulty of estimating
161 the role of all the different factors influencing the palynological data (e.g. pollen productivity
162 and dispersability, source area and distance to sample site, amenability to wind dispersal,
163 deposition and preservation until sampling and analysis of vegetation dynamics) (e.g.
164 (Bradshaw and Webb III, 1985)). Nevertheless, this does not affect our pollen-vegetation
165 relationships as previous work has shown that the pollen percentage variations reflect the
166 past forest cover patterns (Williams and Jackson, 2003) and vegetation composition (Nieto-
167 Lugilde et al., 2015).

168 The interpretation of the pollen diagram was assisted by a constrained hierarchical
169 clustering analysis (CONISS) based on Euclidean distance between samples and applied to
170 the total pollen counting. Analysis was performed in the R environment v. 2.13.2 (R
171 Development Core, 2011) using the `chclust` function from package `Rioja` (Juggins, 2009).

172 We reconstructed paleoclimate for each pollen sample using a Plant Functional Type
173 (PFT) Modern Analogue Technique (MAT) (Mauri et al., 2015) implemented in the R package
174 'Rioja' (Juggins, 2012). The Modern Analogue Technique (MAT) is considered the most

175 suitable method for large-scale climate reconstructions from terrestrial and marine pollen
176 sequences, especially when the training set encompasses a wide range of vegetation and
177 climate zones (Brewer et al., 2007; Juggins and Birks, 2011). In this case, we complied with
178 this assumption using the extensive European Modern Pollen Database (Davis et al., 2013).
179 We reconstructed a range of climate parameters usually estimated from pollen data, namely
180 mean monthly summer (JJA), winter (DJF) and annual temperature and precipitation.

181

182 3.3 Ichnological research

183 This research was based on digital image analysis treatment (Dorador and Rodríguez-
184 Tovar, 2018), on selected cores of IODP Site U1385. The technique is based on image
185 adjustment modifications to enhance ichnoassemblage visualization and characterization.
186 Three adjustment modifications (*levels, brightness and vibrance*) were applied to the high-
187 resolution images using Adobe Photoshop CS6 software[®] for enhancing the visibility of
188 biogenic structures. Ichnotaxonomic identification is mainly based in ichnological
189 observations achieved from cores (Knaust, 2017). In each of these images, ichnofabric
190 attributes (i.e., ichnoassemblage, cross-cutting relationships and degree of bioturbation) are
191 characterized. Quantitative estimation on the percentage of bioturbation was obtained by
192 the application of the Ichnological Digital Analysis Images Package (Dorador and Rodríguez-
193 Tovar, 2018). The amount of bioturbation was characterized and referred to the
194 Bioturbation Index (Taylor and Goldring, 1993).

195

196 3.4 Time series analyses

197 We used REDFIT (Schulz and Mudelsee, 2002) to estimate the Fourier spectrum
198 directly from the unevenly spaced time series of the Mediterranean forest pollen

199 percentages, and we removed the linear trend before estimating the spectrum.. One of the
200 main advantages of REDFIT is that this method is able to separate real signals from the red
201 noise background. To explore potential climate regime shifts contained in the paleoclimate
202 data under analysis, we used the change point method proposed by (Bai and Perron, 2003),
203 as implemented in the R package strucchange (Zeileis A. et al., 2002). This statistical tool
204 identifies the age where there exists a significant structural change in the times series
205 analysed providing the 95% CI (confidence interval) of the change-point, but this tool works
206 only with evenly spaced (“regular”) time series. For this reason, we interpolated the
207 unevenly spaced time series of pollen percentages through Akima method using intervals of
208 200 years. Furthermore, others interval lengths (“100” and “300” years) were used, but the
209 results did not change and are not shown. To estimate the wavelet spectrum to the
210 interpolated pollen percentages (using the same preprocessing strategy such as was
211 described previously) via the Morlet continuous wavelet transform we used the method of
212 (Liu et al., 2007), as implemented in the R package biwavelet (Gouhier and Grinsted, 2014).
213 Please note that it is not necessary to remove a linear trend in the time series of pollen
214 percentages because wavelet spectral analysis is designed to work with non-stationary time
215 series.

216

217 **4. Results**

218 4.1 From pollen-based vegetation changes to westerlies shifts

219 The studied section of U1385 spans the period between 715.2 ka and 672 ka,
220 encompassing the very end of MIS 18, the 38-kyr long MIS 17 (713 - 675 ka), and the very
221 beginning of MIS 16 (Hodell et al., 2015). The sedimentation rate varies between 5.65 and

222 10.09 cm/kyr (Table 1) and the temporal resolution of the pollen analysis is 380-year on
223 average. Pollen diagrams show (Figs. 2 and 3e) a long-term increase of the Mediterranean
224 forest pollen percentages, mainly composed of deciduous *Quercus* and sclerophyllous taxa
225 (evergreen *Quercus*, *Olea*, *Cistus*, *Pistacia* and *Phillyrea*) that tightly follows the gradual
226 changes in summer energy at 65°N (Fig. 3a), defined as the number of summer days in which
227 daily insolation is above 275 W/m² (Huybers, 2006). This parameter integrates the duration
228 and intensity of insolation during the summertime and it is mainly paced by obliquity
229 (Huybers, 2006). Throughout the MIS 17 interglacial, low percentages of sclerophyllous trees
230 and shrubs point to the occurrence of weakly Mediterranean climate compared with other
231 interglacials (Sanchez Goñi et al., 2018), indicating limited seasonality. The two maxima in
232 sclerophyllous plants reveal increased summer warmth and dryness but still high winter
233 precipitation during MIS 17e (~712 ka) and 17c (694 ka) (Fig. 3b and e) and coincide with the
234 two minima in precession that determine stronger seasonality (Meijer and Tuenter, 2007)
235 (Fig. 3a). The terrestrial counterpart of the MIS 17 interglacial *sensu stricto* lasted 27 kyrs
236 (~714-687 ka) in southwestern Iberia according to the criterion used in previous research at
237 the same site (Mediterranean forest pollen >20%, (Sánchez Goñi et al., 2016)). It was
238 followed by a significant forest contraction during MIS 17b and a subsequent forest increase
239 during MIS 17a (~678-673 ka). Superimposed to these orbitally-driven Mediterranean forest
240 changes, time series analyses suggest a succession of forest contractions with dominant 5.2-
241 kyr (90%) and 1-kyr (95%) cyclicities (Figs. 3e, 4 and 5). Quantitative reconstructions of
242 average seasonal and annual temperature and precipitation show a long-term trend
243 characterized by higher winter precipitation during MIS 17e, d and c with a decrease during
244 the second part of this interglacial, MIS 17b and a. During MIS 17c, summer temperature and
245 precipitation records reveal the highest and lowest values, respectively. We recognize that

246 the uncertainties of our quantitative climatic estimations are large, particularly those of
247 winter precipitation, and this is certainly due to the lack of good modern pollen analogues
248 for the MIS 17 interglacial. However, our pollen-based quantitative estimations are in line
249 with present-day vegetation requirements and atmospheric circulation (Gouveia et al., 2008)
250 and, therefore, with our qualitative interpretation. Moreover, in a recent paper (Oliveira et
251 al., 2018) we have clearly shown using a data-model comparison approach that the
252 Mediterranean forest pollen percentage and tree fraction have a strong relationship with
253 winter precipitation.

254 Constrained hierarchical cluster analysis reveals four main pollen zones (Figs. 2 and 3). The
255 first zone, U1385-1 (~715.2-714 ka, MIS 18), falls within the Termination VIII, and is marked
256 by the highest semi-desert pollen percentages (mainly *Artemisia*, Chenopodiaceae and
257 *Ephedra*), indicating that winters were particularly cold and dry with precipitation below
258 present-day values (Fig. 6d and e). The onset of the next pollen zone, U1385-2 (~714-700 ka,
259 MIS 17e-d) is marked by the large and rapid increase of Ericaceae and Mediterranean forest
260 taxa (mainly deciduous *Quercus*, <10%-30%), within 400 years. Today, Ericaceae are
261 abundant in Europe under relatively moist climates with more than 600 mm of annual
262 precipitation, low seasonality, and at least four months of mean temperatures above 10°C
263 (Polunin and Walters, 1985). Our climatic reconstruction indicates a rapid shift to more
264 humid (20mm/month winter and summer increases compared to the previous zone) but still
265 cool conditions (3°C and 19°C in winter and summer, respectively) at ~713 ka (Fig. 6b-e).
266 Ericaceae-dominated shrublands (heathlands) reached its maximum expansion at ~710 ka
267 associated with a moderate increase of deciduous trees and sclerophyllous plants pointing
268 to maximum summer precipitation (up to 50mm/month, i.e. 30mm/month more than at
269 present) by that time (Figs 3d, e and 6c). The significant increase of the Mediterranean forest

270 cover at ~707 ka (Fig. 2), corroborated by the change point method (Fig. S2), indicates a first
271 winter and summer warming (Fig. 6b and e). Summer precipitation remained higher than at
272 present for 15,000 years but winter precipitations slightly decreased. High winter and
273 summer precipitation and moderate warmth during the interval MIS 17e-d (Fig. 6b-e)
274 probably resulted from well-developed Eurasian ice caps (Bintanja and van de Wal, 2008;
275 Hodell et al., 2008). This ice configuration maintained the westerlies and, therefore,
276 precipitation in a southern position comparable, albeit with lesser intensity due to less ice
277 volume, to what is observed and simulated during the last glacial maximum in southern
278 Europe (Lainé et al., 2009; Prentice et al., 1992). A similar heathlands expansion, although
279 with less forest cover, is observed during the last glacial maximum in this region (Turon et
280 al., 2003).

281 At the beginning of pollen zone U1385-3 (~700-692 ka, MIS 17c), Mediterranean
282 forest (>40%; deciduous *Quercus* >30%) replaced heathlands (<15%) (Figs. 2 and 3e),
283 reaching a maximum (up to 78%) at ~696 ka. Modern pollen studies indicate oak forest
284 dominance and heathland presence when deciduous *Quercus* and Ericaceae pollen
285 percentages are above 30% and below 25%, respectively (Huntley and Birks, 1983; Sánchez
286 Goñi and Hannon, 1999). Heathland-dominated landscapes during MIS 17e-d were therefore
287 progressively replaced by the Mediterranean forest. Longer growing seasons favor the
288 development of broad-leaved trees (Kollas et al., 2014) and this particular vegetation change
289 indicates that spring-winter mean temperature progressively increase. This lengthening of
290 the growing season parallels the increase in summer duration, peaking at ~696 ka (Fig. 6a).
291 This interval between ~696 and 694 ka is characterized by the highest mean summer
292 temperatures reaching almost present-day values (22°C, Fig. 6b). Furthermore, mean winter
293 precipitation estimations show that rainfall increased and was again higher than that of the

294 present day. MIS 17c was therefore the period characterized by both maximum summer
295 warmth and dryness and strong influence of the westerlies in this region. It coincides with a
296 strong expansion of the temperate forest in southern Italy (tree pollen percentages of 80%,
297 Montalbano Jonico, 40° 17'N) (Toti, 2015) suggesting that the westerlies substantially
298 affected more eastern and northern regions. A first sharp decrease of the Mediterranean
299 forest in the adjacent landmasses at ~694 ka, pollen percentages from 78% to 60% during
300 the transition MIS 17c/17b, suggests a decrease in winter precipitation, which went under
301 present-day values (Fig. 6e). This shift corresponds with slightly decreasing winter
302 temperatures but still warm summers (Fig. 6d and b). Colder and drier winter conditions
303 compared with MIS 17c suggest a northward shift of the westerlies and their weaker
304 influence in southern Europe at the time of sea level decreasing trend (Fig. 3b). An
305 alternative hypothesis involving a decrease in the amount of moisture transported by the
306 westerlies brought about by the cooling of the subtropical gyre could also explain the
307 dryness recorded at the end of MIS 17c. However, as we will see later, the decrease in the
308 Mediterranean forest and related winter precipitation occurred when the SST in the Iberian
309 margin were still high, between 18 and 20°C. The abundance of *Isoetes* spores notably
310 increased by that time, probably expanding in temporary wetlands established on the
311 coastal areas emerged (Salvo Tierra, 1990) during the contemporary sea level fall.

312 The last pollen zone, U1385-4, encompasses MIS 17b, MIS 17a and the beginning of
313 MIS 16 (~692-673 ka). Its onset is marked by a second sharp decrease of Mediterranean
314 forest pollen (30-40%) at ~692 ka, corroborated by the change point analysis (Fig. S2).
315 Ubiquitous herbs largely increased, inferring a winter climate 2°C colder and 10mm/month
316 drier compared to pollen zone U1385-3 probably amplified by the decrease in summer
317 insolation that follows the decrease in summer energy (Figs. 3c and 6a, d, e). Colder and

318 drier winters in southwestern Iberia suggest a further northward displacement of the
319 westerlies. The second part of this pollen zone, ~686-673 ka, is additionally marked by the
320 increase of heathlands and semi-desert plants and the lowest Mediterranean forest cover of
321 MIS 17 (Fig. 3). These data reveal relatively wet summers, dry winters and a cooler climate
322 during MIS 17b-a (Fig. 6b-e) and we infer a still weaker influence of the westerlies in
323 southwestern Iberia likely related to their sustained northward penetration at the time of ice
324 growth.

325

326 4.2 Local bottom water oxygenation

327 Trace fossils, as reflecting behavior of trace makers, provide detailed information on
328 ecological and depositional parameters; especially, archetypal ichnofacies, as group of
329 biogenic structures that reflect animal responses to paleoenvironmental conditions
330 (MacEachern et al., 2012). Trace fossil assemblage through the studied interval consists of
331 *Planolites* (*Pl*), *Thalassinoides* (*Th*), *Thalassinoides*-like (*Th-l*) structures, and *Zoophycos* (*Zo*)
332 that can be ascribed to the *Zoophycos* ichnofacies, typical of deep sea environments (Figs. 7
333 and S3). These discrete traces are overlapping a mottled background, Bioturbation Index (BI)
334 of 6, associated with biodeformational structures. Abundance of these discrete trace fossils
335 is variable with BI ranging from 1 to 4 (Fig. 7). On this general pattern, significant
336 stratigraphical changes can be observed, allowing differentiation of four ichnofabrics:
337 *Thalassinoides*-like ichnofabric, characterized by dominant *Th-l*, and the presence of *Pl* and
338 *Th*; *Planolites* ichnofabrics, with dominance, near exclusiveness of *Pl*, and light host
339 sediment, *Zoophycos* ichnofabric, with dominant *Zo* and some *Th*, and darker host sediment;
340 and *Thalassinoides* ichnofabric, with dominance of *Th*, and the record of *Pl*. Especially
341 significant is the change between the *Planolites* ichnofabric and the *Zoophycos* ichnofabric at

342 81.43 m, centered at ~693 ka. Dominant/exclusive *Planolites* over a mottled background has
343 been previously interpreted for IODP Site U1385 as bioturbation of uppermost tiers, on or
344 just below the seafloor, associated with relatively good life conditions for macrobenthic
345 trace maker community (oxygenation and nutrients availability) (Rodríguez-Tovar and
346 Dorador, 2014). In this context, absence of deeper tier traces could reveal a relatively high
347 sedimentation rate which avoids the colonization deeper into the sediment. The abrupt
348 appearance of *Zoophycos*, together with *Thalassinoides*, evidences colonization of deeper
349 tiers; this could be related with decreasing in the rate of sedimentation, determining enough
350 time for bioturbation and colonization deeper in the sediment. This time is necessary for
351 development of complex structures such as *Zoophycos*. *Zoophycos* producer has been
352 related to variations in energy, sedimentation rate, food content, or bottom-water
353 oxygenation (Dorador et al., 2016); its relative independence of substrate features would
354 allow for colonization of sediments with comparative low oxygenation (Rodríguez-Tovar and
355 Uchman, 2008). *Zoophycos* is commonly found in hemipelagic sediments deposited during
356 glacial times and when the sedimentation rate was intermediate (from 5 to 20 cm kyr⁻¹) and
357 primary production was high and seasonal (Dorador et al., 2016). Occurrences of *Zoophycos*
358 elsewhere support a similar relationship with seasonal organic-matter deposition. Thus, in
359 the case study, the record of the *Zoophycos* ichnofabric could be related with changes in
360 primary productivity and decreasing in the rate of oxygenation, also supported by the darker
361 colour of the sediment, in a context of higher sedimentation rate. The lightness record from
362 the same IODP site U1385 also shows a substantial change towards higher values in the
363 *Zoophycos* interval (Fig. 7) (Hodell et al., 2013). This strong lightness found in darker
364 sediments could be explained by the abundant bioturbation characterizing this zone and
365 introducing light material in a dark sediment background.

366

367 **5. Discussion**

368 Vegetation-inferred shifts in the westerlies and in local bottom water oxygenation
369 during MIS 17 were compared with sea surface changes in southwestern Iberian margin and
370 other North Atlantic paleoceanographic records located west in the subpolar gyre (ODP Sites
371 646 and 647; IODP Site U1314; ODP Site 984), in the mid-latitude central North Atlantic
372 (IODP Site U1313) and in its easternmost part, off Ireland (ODP Site 980, [Fig. 1](#)). Reduced
373 precipitation at the end of MIS 18 was synchronous with $\delta^{13}C_{37:4}$ -based freshwater pulses
374 and the lowest UK'_{37} -SST in the southwestern Iberian margin (Rodrigues et al., 2017) ([Fig. 8e](#)
375 [and f](#)), as well as the presence of ice rafted debris (IRD) in the subpolar gyre (Alonso-Garcia
376 et al., 2011) indicating that the Subpolar Front and the associated storm tracks (Ogawa et
377 al., 2012), were located at the mid-latitudes of the Iberian margin as far south as below 37°N
378 (Rodrigues et al., 2017) ([Fig. 9](#)). The subsequent 15-kyr long period of sustained summer and
379 winter wetness and annual cool climate between ~713 ka and 700 ka, was associated with
380 warm waters off southwest Iberia, as indicated by UK'_{37} and foraminifera-based SST records
381 from the same site (Martin-Garcia et al., 2015; Rodrigues et al., 2017). During this time
382 interval SSTs in the subpolar-central North Atlantic (U1314) (Alonso-Garcia et al., 2011) and
383 in the western mid-latitude basin (U1313) (Naafs et al., 2011) were the highest of the
384 records and higher than the SST in the northeastern part (ODP 980) ([Fig. 8c](#) and [Fig. S4](#)). This
385 gradient suggests a westward location of the Subpolar Front and deep water formation sites
386 (Alonso-Garcia et al., 2011; Wright and Flower, 2002). The relatively small thermal gradient
387 during the interval from 700 ka to 692 ka between the southern Mg/Ca-based thermocline
388 temperature on *Globorotalia inflata* (U1385, 37°N) and the slightly northern alkenone-based
389 SST record (U1313, 41°N) ([Fig. 8d](#)) additionally suggests a southward position of the

390 thermocline water source of the ENACWsp (Bahr et al., 2018) (Fig. 9). The high amount of
391 winter and summer precipitation in southwestern Europe during MIS 17e-d in comparison
392 with the end of MIS 18 suggests a mid-latitude position of the westerlies during winter and
393 enhanced moisture production during summer giving support to the relative southern
394 position of this warm source region (Bahr et al., 2018) (Fig. 9). Moreover, the dominant 5.2-
395 kyr cyclicity in the Mediterranean forest pollen percentage changes recorded during MIS
396 17e-d-c in the absence of high latitude ice-related freshwater pulses (Alonso-Garcia et al.,
397 2011) (Figs. 4, 5 and 8f) call to the fourth harmonic of precession, i.e. the influence of
398 tropical regions on southwestern Iberian climate (Sánchez Goñi et al., 2016). The reason why
399 low latitudes may lead to millennial-scale changes is due to the fact that they receive, with
400 respect to higher latitudes, twice the maximum amount of daily irradiation over the course
401 of the year (Berger et al., 2006). A direct consequence of this process would be a larger
402 latitudinal thermal gradient and thus enhanced transport of warmth and moisture by either
403 atmospheric (westerlies) or oceanic circulation (subtropical gyre) from equatorial to high
404 latitudes in the North Atlantic (Berger et al., 2006). The arrival of precipitation during winter
405 to a cool Europe allowed the Alpine glaciers, which strongly developed during the 0.8-1.0 Ma
406 time interval (Haeuselmann et al., 2007; Valla et al., 2011), to persist.

407 At the MIS 17d/c transition, centered at ~700 ka, southwestern Iberia warmed up
408 and winter precipitation decreased followed by a sharp increase alongside increasing
409 summer energy (Figs. 5a, f and 7a, g). Bahr et al. (2018) suggested that the thermocline
410 water source of the ENACWsp moved progressively northwards based on the increase in the
411 temperature gradient between IODP sites U1313 and U1385 from 706 ka to 700 ka (Fig. 8d).
412 Other studies show relatively stable SST during MIS 17c in the eastern North Atlantic (ODP
413 980) contemporaneous with a clear decreasing trend westwards (U1314) (Alonso-Garcia et

414 al., 2011; Wright and Flower, 2002) (Fig. 8c). These findings suggested that the Subpolar
415 Front moved to the southeast but allowing the North Atlantic Current (NAC) to enter in the
416 Norwegian Greenland Seas (NGS). This promoted deep water formation in the NGS and
417 brought moisture and warmth towards Northern Hemisphere higher latitudes (Fig. 9).
418 Recent results indicate a change in the circulation regime of the abyssal subtropical North
419 Atlantic, ODP Site 1063 (Fig. 1), during MIS 17 signifying increased production of a dense
420 deepwater mass in the NGS akin to lower North Atlantic deep water in the modern ocean
421 (Poirier and Billups, 2014). This change predated the occurrence of the first deep glacial
422 maximum corresponding to the establishment of strong 100-kyr cycles at ~650 ka (Poirier
423 and Billups, 2014). These findings confirm that the “Nordic heat pump” would have replaced
424 the “Boreal heat pump” at ~700 ka (Imbrie et al., 1993) and additional warmth and moisture
425 were transported to Europe as suggested for the first time by the exceptional forest
426 expansion in southern Europe between ~696 ka and ~694 ka. This interval was marked in
427 this region by the highest annual temperatures of MIS 17 and higher than present winter
428 moisture (Fig. 8g), synchronous, within the age model uncertainties, with particular warm
429 conditions in Greenland according to Barker et al. (2011)’s simulations (Barker et al., 2011)
430 and a peak in CH₄ concentration (Louergue et al., 2008). Likewise, a minimum in ice volume
431 (ice ablation related to high summer energy; (Huybers, 2006)) was then recorded, although
432 moderate-sized ice sheets seem to have persisted compared to other interglacials, as
433 indicated by the $\delta^{18}\text{O}_b$ record (Lisiecki and Raymo, 2005) and the estimated changes in
434 relative sea level (Elderfield et al., 2012) (Fig. 3b). According to Antarctic records, MIS 17 is
435 one of the coolest interglacials of the last 800,000 years (lukewarm interglacial) (Jouzel et al.,
436 2007) marked by the lowest CO₂ and CH₄ concentrations (Louergue et al., 2008; Luthi et al.,
437 2008). Modeling studies have proposed different physical drivers to explain the

438 displacement of winter storm tracks towards southern Europe during the early Holocene
439 (10-8 ka) (Brayshaw et al., 2010), which resembles MIS 17c concerning residual ice caps and
440 Mediterranean forest expansion (Oliveira et al., 2018). By analogy, the regional increase of
441 winter rainfall during MIS 17c could be the result of three factors, low CO₂ concentration,
442 230-240 ppm, low boreal winter insolation that produced stronger Hadley cells and the
443 southern position of North Atlantic storm tracks, and reduced North Atlantic latitudinal
444 gradients of insolation and SST (Morley et al., 2014). These weak gradients are consistent
445 with a reduced requirement for poleward energy from the subtropics to polar latitudes by
446 the storm tracks leading to more zonal winds as shown by the Mediterranean forest
447 expansion (Fig. 8g and 9).

448 During the MIS 17c/17b transition, centered at ~693 ka, the penetration of the
449 westerlies in southern Europe weakened concomitant with still strong warm summers.
450 These conditions indicate a still relatively northward position of the Subpolar Front
451 associated with a major northward shift and intensification of the westerlies. At this time the
452 eastern North Atlantic off Ireland SST slightly increased (ODP 980) reflecting strong influence
453 of NAC water, whereas the western (ODP 647 and U1313), northern (ODP 984) and central
454 (U1314) North Atlantic regions (Alonso-Garcia et al., 2011; Wright and Flower, 2002) got
455 colder, supporting a change in atmospheric conditions in the North Atlantic (Fig. 8c, 9 and
456 Fig. S4). Concomitant with this atmospheric change associated with a drying event in
457 southwestern Iberia, we observe locally the strongest decrease in the rate of oxygenation of
458 the MIS 17 interval (Fig. 6 and Fig. S4) that may be related with the large scale intensification
459 of the deep oceanic currents recorded at that time (Poirier and Billups, 2014). Increased
460 penetration of the westerlies into high latitudes contemporaneous with decreasing summer
461 energy probably amplified ice growth by providing additional moisture. Moreover, the

462 slightly lower *N. pachyderma* (d) $\delta^{18}\text{O}$ values at site U1314 suggest a maximal influence of
463 the NAC in the subpolar gyre during summer (Alonso-Garcia et al., 2011). In this context, the
464 warm waters of the NAC still reached Site U1314 area in summer during glacial inception
465 and this might have introduced additional heat and moisture into the subpolar gyre
466 promoting snow accumulation in colder North America and the surrounding areas. The west-
467 east SST gradient, called “lagging warmth” (Wright and Flower, 2002), persisted during MIS
468 17b and the beginning of MIS 17a associated with intense deep water formation, sustained
469 high $\delta^{13}\text{C}$ values (Alonso-Garcia et al., 2011; Poirier and Billups, 2014), in the NGS
470 additionally fueling glacial inception towards MIS 16. The decrease in summer energy (T275)
471 certainly played an important role in snow production but the westerlies brought the
472 moisture necessary to produce snow and subsequently strong ice accumulation. With this
473 decrease in summer energy, higher latitudes are far too dry to provide the moisture
474 necessary to feed the ice caps. Other processes could amplify the ice accumulation
475 throughout MIS 16 such as the albedo feedback, which reduces ice ablation during this
476 interval of low summer insolation. After the coalescing of the North American ice domes the
477 hysteresis loop permitted a positive ice sheet mass balance through several precession
478 cycles leading to the first strong and long 100-kyr ice age cycle (Abe-Ouchi et al., 2013;
479 Hodell and Channell, 2016).

480

481 **6. Conclusion**

482 The finding that southern Europe was characterized by persistently high winter and
483 summer moisture (twofold today’s precipitation) during the cold summers of the first 15,000
484 years of MIS 17 supports the hypothesis that Europe maintained well-developed Alpine
485 glaciers between ~714 and 700 ka. Our data additionally supports an 18-kyr protacted

486 deglaciation, from ~714 to 696 ka, longer than that modeled, ~6-kyr (Parrenin and Paillard,
487 2012). Between ~700 ka and 694 ka, MIS 17d/17c transition, we infer a significant change in
488 the atmospherically-driven vegetation record with maximum warmth and strong winter
489 moisture in southern Europe concomitant with the progressive intensification of the deep
490 water formation in the NGS and the decrease of the SST latitudinal gradient. The peak of
491 winter precipitation at MIS 17c, ~694 ka, was followed by a pronounced two-steps
492 northward shift and strengthening of the westerlies that would have transported high
493 amount of moisture to higher latitudes, thus amplifying the effect of the arrival of moisture
494 by the warm NAC. This increase of moisture in the northern regions was contemporaneous
495 with a decrease in summer energy and insolation at 65°N that allowed snow fall and
496 subsequent ice sheet growth in colder Greenland, northern Europe and the Arctic during the
497 MIS 17/16 transition, and by hysteresis lead to the final breaking point to the strong 100-kyr
498 ice age cycles.

499

500 ACKNOWLEDGMENTS

501 J.M.P.M. was funded by a Basque Government post-doctoral fellowship and MAG and TR by
502 FCT (PTDC/MAR-PRO/3396/2014, UID/Multi/04326/2013, SFRH/BPD/96960/2013,
503 SFRH/BPD/108600/2015). We acknowledge C. Morales-Molino and D. Oliveira for the
504 reading of the manuscript and V. Hanquiez for drawing Figures 1 and 9. We are grateful to
505 Ludovic Devaux for pollen sample preparation.

506

507 **References**

- 508 Abe-Ouchi, A., Saito, F., Kawamura, K., Raymo, M.E., Okuno, J.i., Takahashi, K., and Blatter,
509 H., 2013, Insolation-driven 100,000-year glacial cycles and hysteresis of ice-sheet
510 volume: *Nature*, v. 500, p. 190.
- 511 Alonso-Garcia, M., Sierro, F.J., Kucera, M., Flores, J.A., Cacho, I., and Andersen, N., 2011,
512 Ocean circulation, ice sheet growth and interhemispheric coupling of millennial
513 climate variability during the mid-Pleistocene (ca 800–400 ka): *Quaternary*
514 *Science Reviews*, v. 30, p. 3234-3247.
- 515 Bahr, A., Kaboth, S., Hodell, D., Zeeden, C., Fiebig, J., and Friedrich, O., 2018, Oceanic heat
516 pulses fueling moisture transport towards continental Europe across the mid-
517 Pleistocene transition: *Quaternary Science Reviews*, v. 179, p. 48-58.
- 518 Bai, J., and Perron, P., 2003, Computation and analysis of multiple structural change models:
519 *Journal of Applied Econometrics*, v. 18, p. 1-22.
- 520 Barker, S., Knorr, G., Edwards, R.L., Parrenin, F., Putnam, A.E., Skinner, L.C., Wolff, E., and
521 Ziegler, M., 2011, 800,000 Years of Abrupt Climate Variability: *Science*.
- 522 Berger, A., and Loutre, M.F., 1991, Insolation values for the climate of the last 10 million
523 years: *Quaternary Science Reviews*, v. 10, p. 297-317.
- 524 Berger, A., Loutre, M.F., and Mélice, J.L., 2006, Equatorial insolation: from precession
525 harmonics to eccentricity frequencies: *Clim. Past*, v. 2, p. 131-136.
- 526 Bintanja, R., and van de Wal, R.S.W., 2008, North American ice-sheet dynamics and the
527 onset of 100,000-year glacial cycles: *Nature*, v. 454, p. 869.

- 528 Blanco Castro, E., Casado González, M.A., Costa Tenorio, M., Escribano Bombín, R., García
529 Antón, M., Génova Fuster, M., Gómez Manzaneque, F., Moreno Sáiz, J.C., Morla
530 Juaristi, C., Regato Pajares, P., and Sáiz Ollero, H., 1997, *Los bosques ibéricos:*
531 *Barcelona, Planeta, 572 p.*
- 532 Bradshaw, R.H.V., and Webb III, T., 1985, Relationships between contemporary pollen and
533 vegetation data from Wisconsin and Michigan, USA.: *Ecology*, v. 66, p. 721-737.
- 534 Brayshaw, D.J., Hoskins, B., and Black, E., 2010, Some physical drivers of changes in the
535 winter storm tracks over the North Atlantic and Mediterranean during the Holocene:
536 *Philosophical Transactions of the Royal Society A*, v. 368, p. 5185-5223.
- 537 Brewer, S., Guiot, J., and Barboni, D., 2007, Pollen data as climate proxies, *in* Elias, S.A., ed.,
538 *Encyclopedia of Quaternary Science*, Elsevier, p. 2498-2510.
- 539 Davis, B.A.S., Zanon, M., Collins, P., Mauri, A., Bakker, J., Barboni, D., Barthelmes, A.,
540 Beaudouin, C., Bjune, A.E., Bozilova, E., Bradshaw, R.H.W., Brayshay, B.A., Brewer, S.,
541 Brugiapaglia, E., Bunting, J., Connor, S.E., de Beaulieu, J.-L., Edwards, K., Ejarque, A.,
542 Fall, P., Florenzano, A., Fyfe, R., Galop, D., Giardini, M., Giesecke, T., Grant, M.J.,
543 Guiot, J., Jahns, S., Jankovská, V., Juggins, S., Kahrmann, M., Karpińska-Kończak, M.,
544 Kończak, P., Köhl, N., Kuneš, P., Lapteva, E.G., Leroy, S.A.G., Leydet, M., Guiot, J.,
545 López Sáez, J.A., Masi, A., Matthias, I., Mazier, F., Meltsov, V., Mercuri, A.M., Miras,
546 Y., Mitchell, F.J.G., Morris, J.L., Naughton, F., Nielsen, A.B., Novenko, E., Odgaard, B.,
547 Ortu, E., Overballe-Petersen, M.V., Pardoe, H.S., Peglar, S.M., Pidek, I.A., Sadori, L.,
548 Seppä, H., Severova, E., Shaw, H., Święta-Musznicka, J., Theuerkauf, M., Tonkov, S.,
549 Veski, S., van der Knaap, W.O., van Leeuwen, J.F.N., Woodbridge, J., Zimny, M., and

- 550 Kaplan, J.O., 2013, The European Modern Pollen Database (EMPD) project:
551 Vegetation History and Archaeobotany, v. 22, p. 521-530.
- 552 Dorador, J., and Rodríguez-Tovar, F.J., 2018, High-resolution image treatment in ichnological
553 core analysis: Initial steps, advances and prospects: Earth-Sciences Reviews, v. 177, p.
554 226-237.
- 555 Dorador, J., Wetzel, A., and Rodríguez-Tovar, F.J., 2016, Zoophycos in deep-sea sediments
556 indicates high and seasonal primary productivity: ichnology as a proxy in
557 palaeoceanography during glacial-interglacial variations: Terra Nova, v. 28, p. 323-
558 328.
- 559 Ehlers, J., and Gibbard, P.L., 2007, The extent and chronology of Cenozoic Global Glaciation:
560 Quaternary International, v. 164-165, p. 6-20.
- 561 Elderfield, H., Ferretti, P., Greaves, M., Crowhurst, S., McCave, I.N., Hodell, D., and
562 Piotrowski, A.M., 2012, Evolution of Ocean Temperature and Ice Volume Through the
563 Mid-Pleistocene Climate Transition: Science, v. 337, p. 704-709.
- 564 Fiúza, A.F.d.G., Macedo, M.E.d., and Guerreiro, M.R., 1982, Climatological space and time
565 variation of the Portuguese coastal upwelling: Oceanologica Acta, v. 5, p. 31-40.
- 566 Fletcher, W.J., and Sanchez Goñi, M.F., 2008, Orbital- and sub-orbital-scale climate impacts
567 on vegetation of the western
568 Mediterranean basin over the last 48,000 yr: Quaternary Research, v. 70 p. 451-464.
- 569 Gouhier, T.C., and Grinsted, A., 2014, Package 'biwavelet': R Package Version 0.20.11.

- 570 Gouveia, C., Trigo, R.M., DaCamara, C.C., Libonati, R., and Pereira, J.M.C., 2008, The North
571 Atlantic Oscillation and European vegetation dynamics: *International Journal of*
572 *Climatology*, v. 28, p. 1835-1847.
- 573 Haeuselmann, P., Granger, D.E., Jeannin, P.-Y., and Lauritzen, S.-E., 2007, Abrupt glacial
574 valley incision at 0.8 Ma dated from cave deposits in Switzerland: *Geology*, v. 35, p.
575 143-146.
- 576 Hodell, D., Crowhurst, S., Skinner, L., Tzedakis, P.C., Margari, V., Channell, J.E.T., Kamenov,
577 G., Maclachlan, S., and Rothwell, G., 2013, Response of Iberian Margin sediments to
578 orbital and suborbital forcing over the past 420 ka: *Paleoceanography*, v. 28, p. 185-
579 199.
- 580 Hodell, D.A., and Channell, J.E.T., 2016, Mode transitions in Northern Hemisphere glaciation:
581 co-evolution of millennial and orbital variability in Quaternary climate: *Clim. Past*, v.
582 12, p. 1805-1828.
- 583 Hodell, D.A., Channell, J.E.T., Curtis, J.H., Romero, O.E., and Röhl, U., 2008, Onset of “Hudson
584 Strait” Heinrich events in the eastern North Atlantic at the end of the middle
585 Pleistocene transition (~640 ka)?: *Paleoceanography*, v. 23, p. PA4218.
- 586 Hodell, D.A., Lourens, L., Crowhurst, S., Konijnendijk, Tjallingii, R., Jiménez-Espejo, F.,
587 Skinner, L., Tzedakis, P.C., and Members, S.S.P., 2015, A reference time scale for site
588 U1385 (Shackleton Site) on the Iberian Margin: *Global and Planetary Change*, v. 133,
589 p. 49-64.
- 590 Huntley, B., and Birks, H.J.B., 1983, *An Atlas of Past and Present Pollenmaps for Europe: 0-*
591 *13.000 B.P. years ago*: Cambridge, Cambridge University Press, 667 p.

- 592 Huybers, P., 2006, Early Pleistocene Glacial Cycles and the Integrated Summer Insolation
593 Forcing: Science.
- 594 Imbrie, J., Berger, A., Boyle, E.A., Clemens, S.C., Duffy, A., Howard, W.R., Kukla, G.J.,
595 Kutzbach, J., Martinson, D.G., McIntyre, A., Mix, A.C., Molino, B., Morley, J.J.,
596 Peterson, L.C., Pisias, N.G., Prell, W.L., Raymo, M.E., Shackleton, N.J., and Toggweiler,
597 J.R., 1993, On the structure and origin of major glaciation cycles 2. The 100,000-year
598 cycle: *Paleoceanography*, v. 8, p. 699-735.
- 599 Jouzel, J., Masson-Delmotte, V., Cattani, O., Dreyfus, G., Falourd, S., Hoffmann, G., Minster,
600 B., Nouet, J., Barnola, J.M., Chappellaz, J., Fischer, H., Gallet, J.C., Johnsen, S.,
601 Leuenberger, M., Loulergue, L., Luethi, D., Oerter, H., Parrenin, F., Raisbeck, G.,
602 Raynaud, D., Schilt, A., Schwander, J., Selmo, E., Souchez, R., Spahni, R., Stauffer, B.,
603 Steffensen, J.P., Stenni, B., Stocker, T.F., Tison, J.L., Werner, M., and Wolff, E.W.,
604 2007, Orbital and Millennial Antarctic Climate Variability over the Past 800,000 Years:
605 *Science*, v. 317 p. 793-796.
- 606 Juggins, S., 2009, Package "rioja" - Analysis of Quaternary Science Data, The Comprehensive
607 R Archive Network.
- 608 —, 2012, Rioja: Analysis of Quaternary Science Data. R package version (0.8-3).
- 609 Juggins, S., and Birks, H.J.B., 2011, Quantitative environmental reconstructions from
610 biological data, *in* Birks, H.J.B., Lotter, A.F., Juggins, S., and Smol, J.P., eds., *Tracking
611 Environmental Change Using Lake Sediments: Data Handling and
612 Numerical Techniques*, Springer, p. 431-494.

- 613 Knaust, D., 2017, Atlas of Trace Fossils in Well Core: Appearance, Taxonomy and
614 Interpretation: Cham, Switzerland, Springer.
- 615 Kollas, C., Körner, C., and Randin, C.F., 2014, Spring frost and growing season length co-
616 control the cold range limits of broad-leaved trees: *Journal of Biogeography*, v. 41, p.
617 773-783.
- 618 Laîné, A., Kageyama, M., Salas-Mélia, D., Voldoire, A., Rivière, G., Ramstein, G., Planton, S.,
619 Tyteca, S., and Peterschmitt, J.Y., 2009, Northern hemisphere storm tracks during the
620 last glacial maximum in the PMIP2 ocean-atmosphere coupled models: energetic
621 study, seasonal cycle, precipitation: *Climate Dynamics*, v. 32, p. 593-614.
- 622 Lisiecki, L., and Raymo, M.E., 2005, A Pliocene-Pleistocene stack of 57 globally distributed
623 benthic $\delta^{18}\text{O}$ records: *Paleoceanography*, v. 20, p. PA1003.
- 624 Liu, Y., San Liang, X., and Weisberg, R.H., 2007, Rectification of the bias in the wavelet power
625 spectrum: *Journal of Atmospheric and Oceanic Technology*, v. 24, p. 2093-102.
- 626 Loulergue, L., Schilt, A., Spahni, R., Masson-Delmotte, V., Blunier, T., Lemieux, B., Barnola, J.-
627 M., Raynaud, D., Stocker, T.F., and Chappellaz, J., 2008, Orbital and millennial-scale
628 features of atmospheric CH_4 over the past 800,000[thinsp]years: *Nature*, v. 453, p.
629 383-386.
- 630 Luthi, D., Le Floch, M., Bereiter, B., Blunier, T., Barnola, J.-M., Siegenthaler, U., Raynaud, D.,
631 Jouzel, J., Fischer, H., Kawamura, K., and Stocker, T.F., 2008, High-resolution carbon
632 dioxide concentration record 650,000-800,000[thinsp]years before present: *Nature*,
633 v. 453, p. 379-382.

- 634 MacEachern, J.A., Bann, K.L., Gingras, M.K., Zonneveld, J.P., Dashtgard, S.L., and Pemberton,
635 G., 2012, The ichnofacies paradigm, *in* Knaust, D., and Bromley, R.G., eds., Trace
636 fossils as indicators of sedimentary environments: Developments in Sedimentology,
637 Volume 64, Elsevier, p. 103-138.
- 638 Marchal, O., Waelbroeck, C., and Verdière, A.C.d., 2016, On the Movements of the North
639 Atlantic Subpolar Front in the Preinstrumental Past: *Journal of Climate*, v. 29, p. 1545-
640 1571.
- 641 Martin-Garcia, G.M., Alonso-Garcia, M., Sierro, F.J., Hodell, D.A., and Flores, J.A., 2015,
642 Severe cooling episodes at the onset of deglaciations on the Southwestern Iberian
643 margin from MIS 21 to 13 (IODP site U1385): *Global and Planetary Change*, v. 135, p.
644 159-169.
- 645 Mauri, A., Davis, B.A.S., Collins, P.M., and Kaplan, J.O., 2015, The climate of Europe during
646 the Holocene: a gridded pollen-based reconstruction and its multi-proxy evaluation:
647 *Quaternary Science Reviews*, v. 112, p. 109-127.
- 648 Meijer, P.T., and Tuenter, E., 2007, The effect of precession-induced changes in the
649 Mediterranean freshwater budget on circulation at shallow and intermediate depth:
650 *Journal of Marine Systems*, v. 68, p. 349-365.
- 651 Miranda, P.M.A., Coelho, F.E.S., Tomé, A.R., Valente, M.A., Carvalho, A., Pires, C., Pires, H.O.,
652 Pires, V.C., and Ramalho, C., 2002, 20th century Portuguese Climate and Climate
653 Scenarios, *in* Santos, F.D., Forbes, K., and Moita, R., eds., *Climate Change in Portugal:
654 Scenarios, Impacts and Adaptation Measures (SIAM Project)*: Gradiva, p. 23-83.

- 655 Morley, A., Rosenthal, Y., and deMenocal, P., 2014, Ocean-atmosphere climate shift during
656 the mid-to-late Holocene transition: *Earth and Planetary Science Letters*, v. 388, p.
657 18-26.
- 658 Mudelsee, M., and Stattegger, K., 1997, Exploring the structure of the mid-Pleistocene
659 revolution with advanced methods of time-series analysis: *Geologische Rundschau*, v.
660 86, p. 499-511.
- 661 Naafs, B.D.A., Hefter, J., Ferretti, P., Stein, R., and Haug, G.H., 2011, Sea surface
662 temperatures did not control the first occurrence of Hudson Strait Heinrich Events
663 during MIS 16: *Paleoceanography*, v. 26, p. PA4201.
- 664 Naafs, B.D.A., Hefter, J., and Stein, R., 2013, Millennial-scale ice rafting events and Hudson
665 Strait Heinrich(-like) Events during the late Pliocene and Pleistocene: a review:
666 *Quaternary Science Reviews*, v. 80, p. 1-28.
- 667 Nieto-Lugilde, D., Maguire, K.C., Blois, J.L., Williams, J.W., and Fitzpatrick, M.C., 2015, Close
668 agreement between pollen-based and forest inventory-based models of vegetation
669 turnover: *Global Ecology and Biogeography*.
- 670 Ogawa, F., Nakamura, H., Nishii, K., Miyasaka, T., and Kuwano-Yoshida, A., 2012,
671 Dependence of the climatological axial latitudes of the tropospheric westerlies and
672 storm tracks on the latitude of an extratropical oceanic front: *Geophysical Research*
673 *Letters*, v. 39.
- 674 Oliveira, D., Desprat, S., Yin, Q., Naughton, F., Trigo, R., Rodrigues, T., Abrantes, F., and
675 Sánchez Goñi, M.F., 2018, Unraveling the forcings controlling the vegetation and

- 676 climate of the best orbital analogues for the present interglacial in SW Europe:
677 Climate Dynamics, v. 51, p. 667-686.
- 678 Parrenin, F., and Paillard, D., 2012, Terminations VI and VIII (~530 and ~720 kyr BP) tell us
679 the importance of obliquity and precession in the triggering of deglaciations: Clim.
680 Past, v. 8, p. 2031-2037.
- 681 Poirier, R.K., and Billups, K., 2014, The intensification of northern component deepwater
682 formation during the mid-Pleistocene climate transition: Paleoceanography, v. 29, p.
683 1046-1061.
- 684 Polunin, O., and Walters, M., 1985, A guide to the vegetation of Britain and Europe: New
685 York, Oxford University Press, 238 p.
- 686 Prentice, I.C., Guiot, J., and Harrison, S.P., 1992, Mediterranean vegetation, lake levels and
687 palaeoclimate at the Last Glacial Maximum: Nature, v. 360, p. 658.
- 688 R Development Core, T., 2011, R: A language and environment for statistical computing:
689 Vienna, Austria, R Foundation for Statistical Computing.
- 690 Railsback, L.B., Gibbard, P.L., Head, M.J., Voarintsoa, N.R.G., and Toucanne, S., 2015, An
691 optimized scheme of lettered marine isotope substages for the last 1.0 million years,
692 and the climatostratigraphic nature of isotope stages and substages: Quaternary
693 Science Reviews, v. 111, p. 94-106.
- 694 Ramos, A., Trigo, R.M., and Santo, F.E., 2011, Evolution of extreme temperatures in Portugal:
695 reporting on recent changes and future scenarios: Climate Research, v. 48, p. 177-
696 192.

- 697 Ríos, A.F., Pérez, F.F., and Fraga, F., 1992, Water masses in the upper and middle North
698 Atlantic Ocean east of the Azores: Deep Sea Research Part A. Oceanographic
699 Research Papers, v. 39, p. 645-658.
- 700 Rodrigues, T., Alonso-García, M., Hodell, D.A., Rufino, M., Naughton, F., Grimalt, J.O.,
701 Voelker, A.H.L., and Abrantes, F., 2017, A 1-Ma record of sea surface temperature
702 and extreme cooling events in the North Atlantic: A perspective from the Iberian
703 Margin: Quaternary Science Reviews, v. 172, p. 118-130.
- 704 Rodríguez-Tovar, F.J., and Dorador, J., 2014, Ichnological analysis of Pleistocene sediments
705 from the IODP Site U1385 "Shackleton Site" on the Iberian margin: Approaching
706 paleoenvironmental conditions: Palaeogeography, Palaeoclimatology, Palaeoecology,
707 v. 409, p. 24-32.
- 708 Rodríguez-Tovar, F.J., and Uchman, A., 2008, Bioturbational disturbance of the Cretaceous-
709 Palaeogene (K-Pg) boundary layer: Implications for the interpretation of the K-Pg
710 boundary impact event: Geobios, v. 41, p. 661-667.
- 711 Salvo Tierra, E., 1990, Guía de helechos de la Península Ibérica y Baleares: Madrid.
- 712 Sanchez Goñi, M.F., Desprat, S., Fletcher, W.J., Morales del Molino, C., Naughton, F., Oliveira,
713 D., Urrego, D.H., and Zorzi, C., 2018, Pollen from the deep-sea: a breakthrough in the
714 mystery of the Ice Ages: Frontiers in Plant Science, v. 9.
- 715 Sánchez Goñi, M.F., and Hannon, G., 1999, High altitude vegetational patterns on the Iberian
716 Mountain chain (north-central Spain) during the Holocene: The Holocene, v. 9, p. 39-
717 57.

- 718 Sánchez Goñi, M.F., Rodrigues, T., Hodell, D.A., Polanco-Martínez, J.M., Alonso-García, M.,
719 Hernández-Almeida, I., Desprat, S., and Ferretti, P., 2016, Tropically-driven climate
720 shifts in southwestern Europe during MIS 19, a low eccentricity interglacial: *Earth and*
721 *Planetary Science Letters*, v. 448, p. 81-93.
- 722 Schulz, M., and Mudelsee, M., 2002, REDFIT: estimating red-noise spectra directly from
723 unevenly spaced paleoclimatic time series. : *Computers & Geosciences*, v. 28, p. 421-
724 426.
- 725 Stow, D.A.V., Hernández-Molina, F.J., Alvarez Zarikian, C.A., and Scientists, t.E., 2013,
726 *Proceedings IODP, 339, Tokyo (Integrated Ocean Drilling Program Management*
727 *International, Inc.)*.
- 728 Taylor, A., and Goldring, R., 1993, Description and analysis of bioturbation and ichnofabric:
729 *Journal of the Geological Society of London*, v. 150, p. 141-148.
- 730 Toti, F., 2015, Interglacial vegetation patterns at the early-middle Pleistocene transition: a
731 point of view from the Montalbano Jonico section (Southern Italy): *Alpine and*
732 *Mediterranean Quaternary*, p. 131-143.
- 733 Turon, J.-L., Lézine, A.-M., and Denèfle, M., 2003, Land-sea correlations for the last glaciation
734 inferred from a pollen and dinocyst record from the Portuguese margin: *Quaternary*
735 *Research*, v. 59, p. 88-96.
- 736 Valla, P.G., Shuster, D.L., and van der Beek, P.A., 2011, Significant increase in relief of the
737 European Alps during mid-Pleistocene glaciations: *Nature Geoscience*, v. 4, p. 688.
- 738 Williams, J.W., and Jackson, S.T., 2003, Palynological and AVHRR observations of modern
739 vegetational gradients in eastern North America: *The Holocene*, v. 13, p. 485-497.

740 Wright, A.K., and Flower, B.P., 2002, Surface and deep ocean circulation in the subpolar
741 North Atlantic during the mid-Pleistocene revolution: *Paleoceanography*, v. 17, p. 20-
742 1-20-16.

743 Zeileis A., Leisch, F., Hornik, K., and Kleiber, C., 2002, Strucchange: an R package for testing
744 for structural change in linear regression models: *Journal of statistical software*, v. 7,
745 p. 1-38.

746

747 **Table legends**

748 Table 1. Control points used to establish by linear interpolation the age model of the interval
749 MIS 17 in IODP Site U1385. The age model is based on the LR04 stack (Lisiecki and Raymo,
750 2005).

751 **Figure legends**

752 Figure 1 – Map with the sites discussed in the text. The position of the present-day Subpolar
753 Front follows approximately the 10°C isotherm (Marchal et al., 2016). STG: Subtropical gyre,
754 AZ: Azores Current, PC: Portuguese Current; SPG: Subpolar gyre; NC: Norwegian Current.
755 Red and blue arrows indicate the northward and zonal path of the westerlies, respectively.

756 Figure 2 - Detailed pollen diagram with selected taxa and ecological groups. On the right side
757 we show the four main pollen zones identified by the constrained hierarchical cluster
758 analysis (CONISS).

759 Figure 3 – Pollen-inferred vegetation changes during MIS 17 in southwestern Iberia, along
760 with changes in ice volume and orbital forcing: a) Summer energy (green line), T275 defines

761 the number of summer days in which daily insolation is above 275 W/m^2 (Huybers, 2006),
762 July insolation at 65°N (black line), precession index (red line) and obliquity (blue line)
763 (Berger and Loutre, 1991). b) Low and high resolution $\delta^{18}\text{O}_b$ profiles from IODP sites U1385
764 (black line) (Hodell et al., 2015) and U1308 (grey line) (Hodell and Channell, 2016)
765 respectively, and relative sea level curve (stippled line) (Elderfield et al., 2012). c-e) Pollen
766 percentages of the most relevant plant taxa and ecological groups (IODP site U1385). The
767 position of MIS 17a-e sub-stages follows Railsback et al. (2015). Numbers 1 to 4 indicate the
768 four main pollen zones. Dashed lines indicate the significant onset of the major pollen zones.
769 Long arrows in panel e depict the 5.2-kyr cyclicity of forest contractions. Grey bar represents
770 the interval with the maximum development of the Mediterranean forest. Blue bars denote
771 MIS 18 and MIS 16.

772 Figure 4 - Wavelet spectrum via the Morlet continuous wavelet transform computed for the
773 time series of Mediterranean forest pollen percentages. A strong signal around 5,000-years
774 dominates a large part of the MIS 17 interglacial. The solid black contour encloses regions of
775 $\geq 80\%$ confidence.

776 Figure 5. Spectral analysis based on REDFIT. This analysis identifies two dominant cyclicities,
777 at 5,200 years (90%) and at 1,000 years (95%).

778 Figure 6 – Pollen-based quantitative climatic reconstructions for southwestern Europe
779 during MIS 17 and orbital forcing: a) Summer energy (green line) (Huybers, 2006), July
780 insolation at 65°N (black line) (Berger and Loutre, 1991). b-d) Summer, June-August, and
781 winter, December-February, temperature reconstructions (dark grey), and 5-point weighted
782 average curve (red). c-e) summer, June- August, and winter, December-February,
783 precipitation reconstructions (dark grey) and 5-point weighted average curve (purple). f)

784 Pollen percentages of Mediterranean forest (mainly deciduous and evergreen *Quercus*, *Olea*,
785 *Pistacia*, *Phillyrea*, *Cistus*) and Ericaceae. Grey shadow indicates the minimum and maximum
786 standard errors that are the uncertainties calculated by the transfer function (Mauri et al.,
787 2015) . Dashed lines are present-day (1961-1990) temperature and precipitation from
788 southwest Portugal (Miranda et al., 2002; Ramos et al., 2011). Blue bands show MIS 18 and
789 MIS 16 glacial periods. Grey band represents the pollen zone U1385-3. The position of MIS
790 17a-e sub-stages follows Railsback et al. (2015). Present-day climate refers to the 1961-1990
791 period.

792 Figure 7 - Ichnological features in the interval 695.15-677.77 ka, showing the distribution of
793 the differentiated ichnofabrics, and dominant ichnotaxa (Pl, *Planolites*; Th,
794 *Thalassinoides*; Th-l, *Thalassinoides*-like, Zo, *Zoophycos*). BI = Bioturbation Index. On the right
795 side, the high resolution lightness record (L^*) from the same IODP Site U1385 (Hodell et al.,
796 2015).

797 Figure 8 – Changes in atmospheric circulation in southwestern Europe inferred from pollen
798 data, compared with orbital forcing, ice volume and oceanographic changes: a) Summer
799 energy (green line) and July insolation at 65°N (black line), b) Low and high resolution $\delta^{18}O_b$
800 profiles from IODP sites U1385 (black line) (Hodell et al., 2015) and U1308 (grey line) (Hodell
801 and Channell, 2016), respectively, c) Sea Surface Temperatures (SST) in the north-central
802 (U1314) and north-eastern (ODP 980) North Atlantic (Alonso-Garcia et al., 2011; Wright and
803 Flower, 2002). d) Thermal gradient between IODP sites U1385 and U1313 (Bahr et al., 2018).
804 e) Foraminifera (pink triangles)- and Uk'37 (purple circles)-based SST records from the IODP
805 site U1385 (Martin-Garcia et al., 2015; Rodrigues et al., 2017). f) Freshwater pulses in the
806 Iberian margin based on the $C_{37:4}$ record of the IODP site U1385 (Rodrigues et al., 2017). g) g)

807 Pollen based mean annual temperature and winter precipitation records in southwestern
808 Iberia (IODP site U1385; this study). Decreases in winter precipitation in southwestern Iberia
809 during the MIS 17 interglacial indicates northward shift of the westerlies. * Present-day
810 winter precipitation. Note that these estimations have large uncertainties (see Figure 6).
811 Nevertheless, the long-term changes in the average quantitative temperature and
812 precipitation reconstructions agree with the qualitative interpretation of the pollen record.

813 Figure 9 – Schematic overview of the atmospheric and oceanic processes evolving during
814 MIS 17. Arrows indicate the position of the westerlies. Red circles: warm SST, blue circles:
815 cold SST, grey circles: no SST data. Pink dashed area indicates the position of the deep water
816 formation.

817

Figure 1
[Click here to download high resolution image](#)

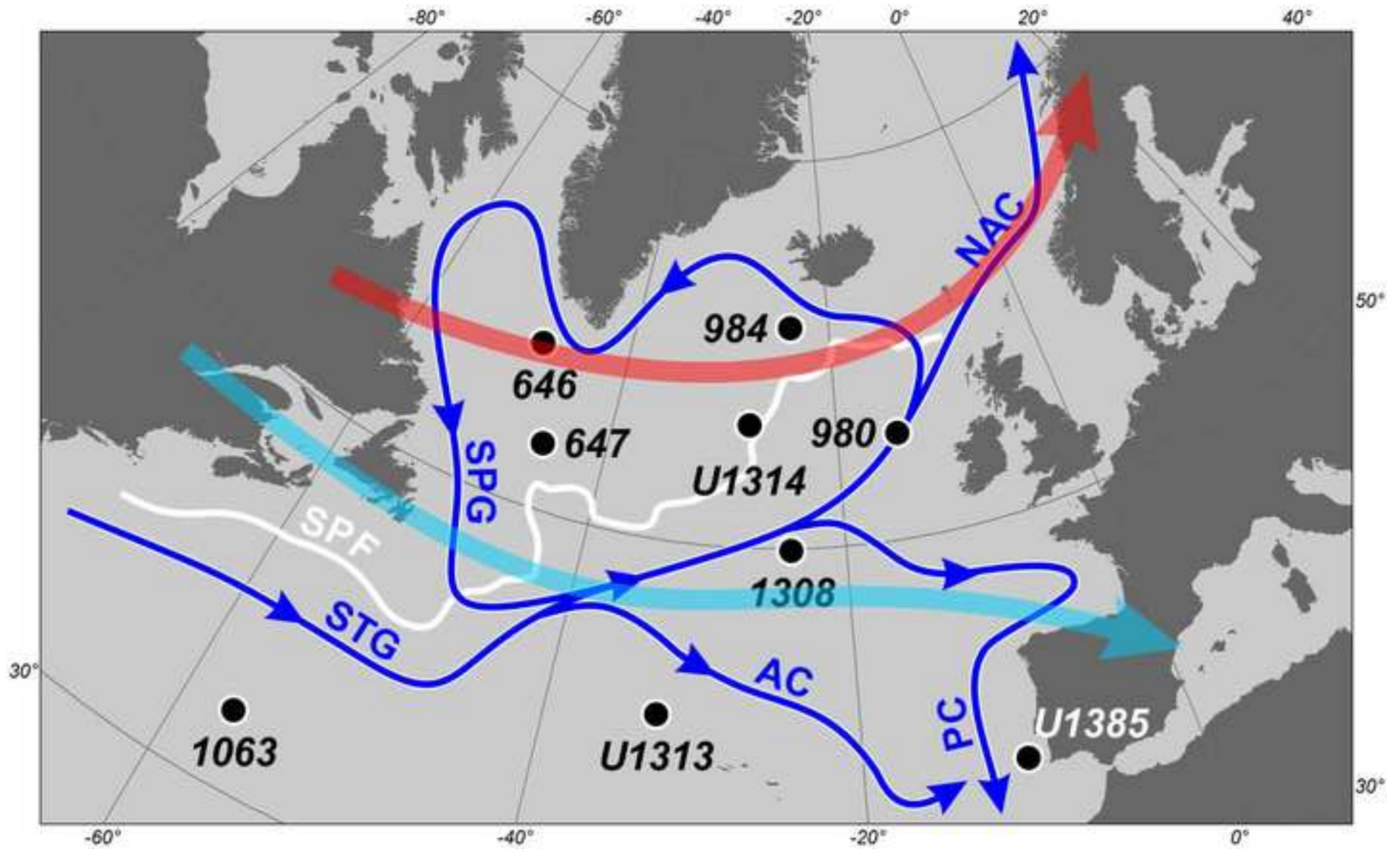


Figure 2
[Click here to download high resolution image](#)

U1385-MIS 17

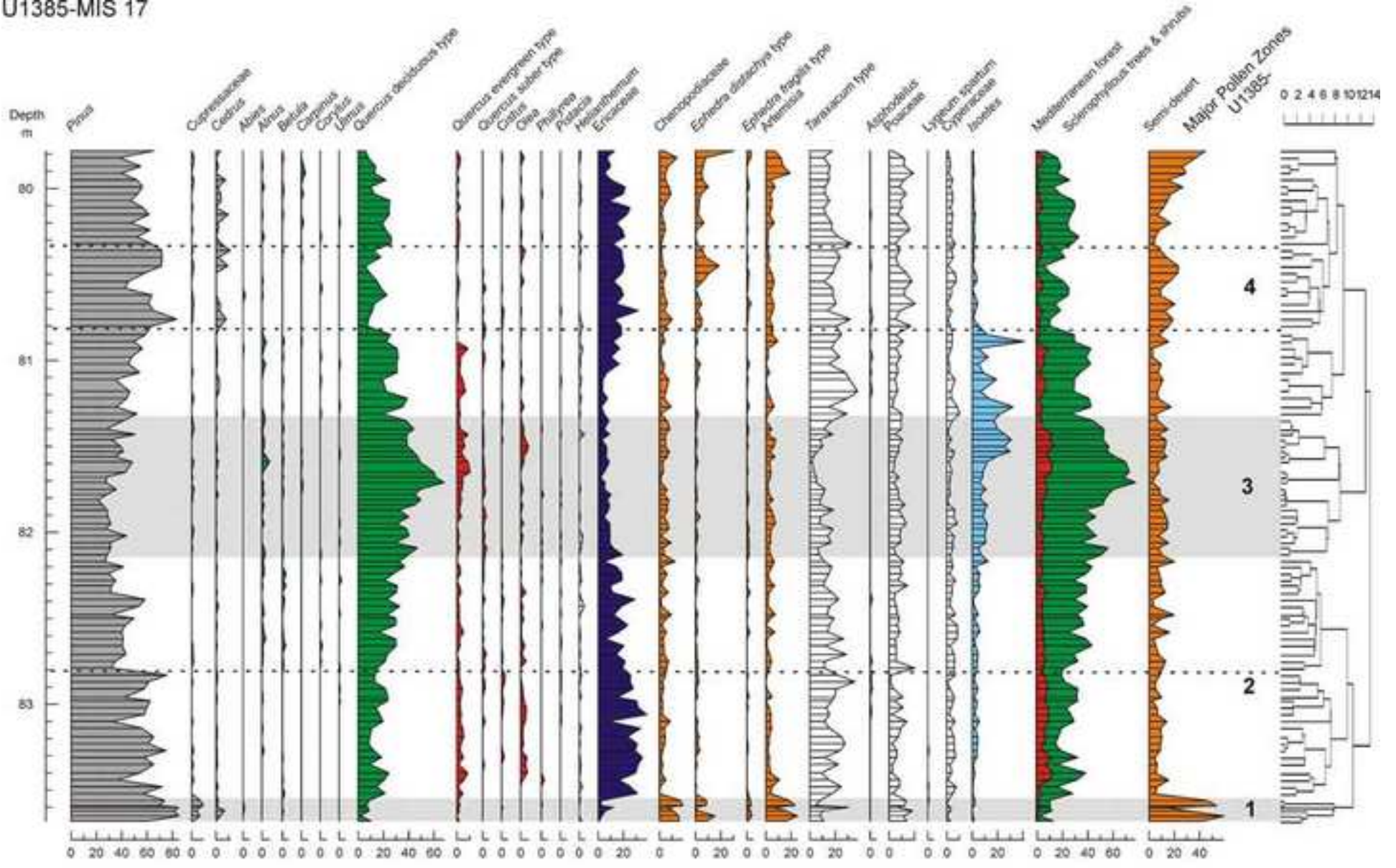


Figure 3
[Click here to download high resolution image](#)

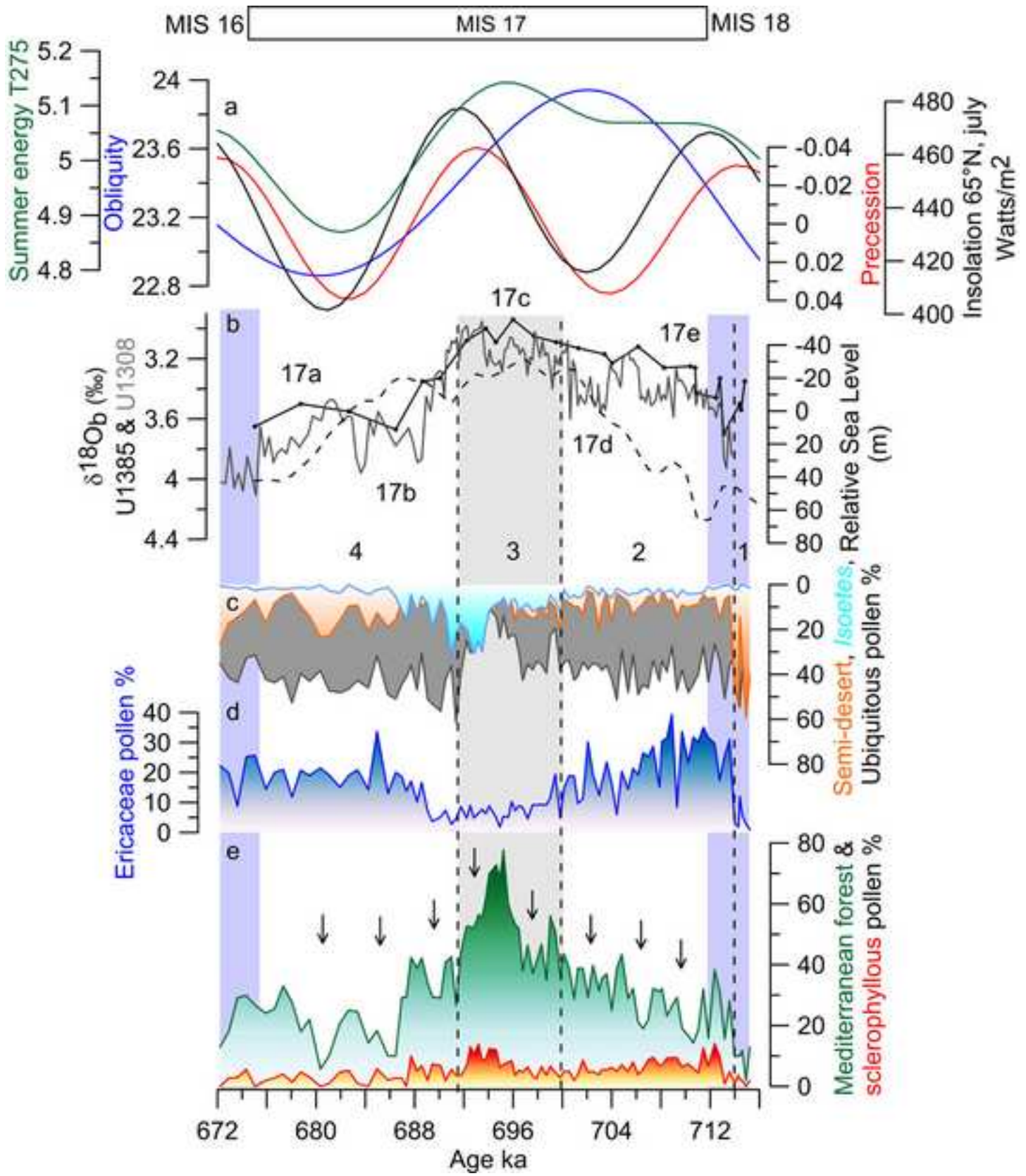


Figure 4
[Click here to download high resolution image](#)

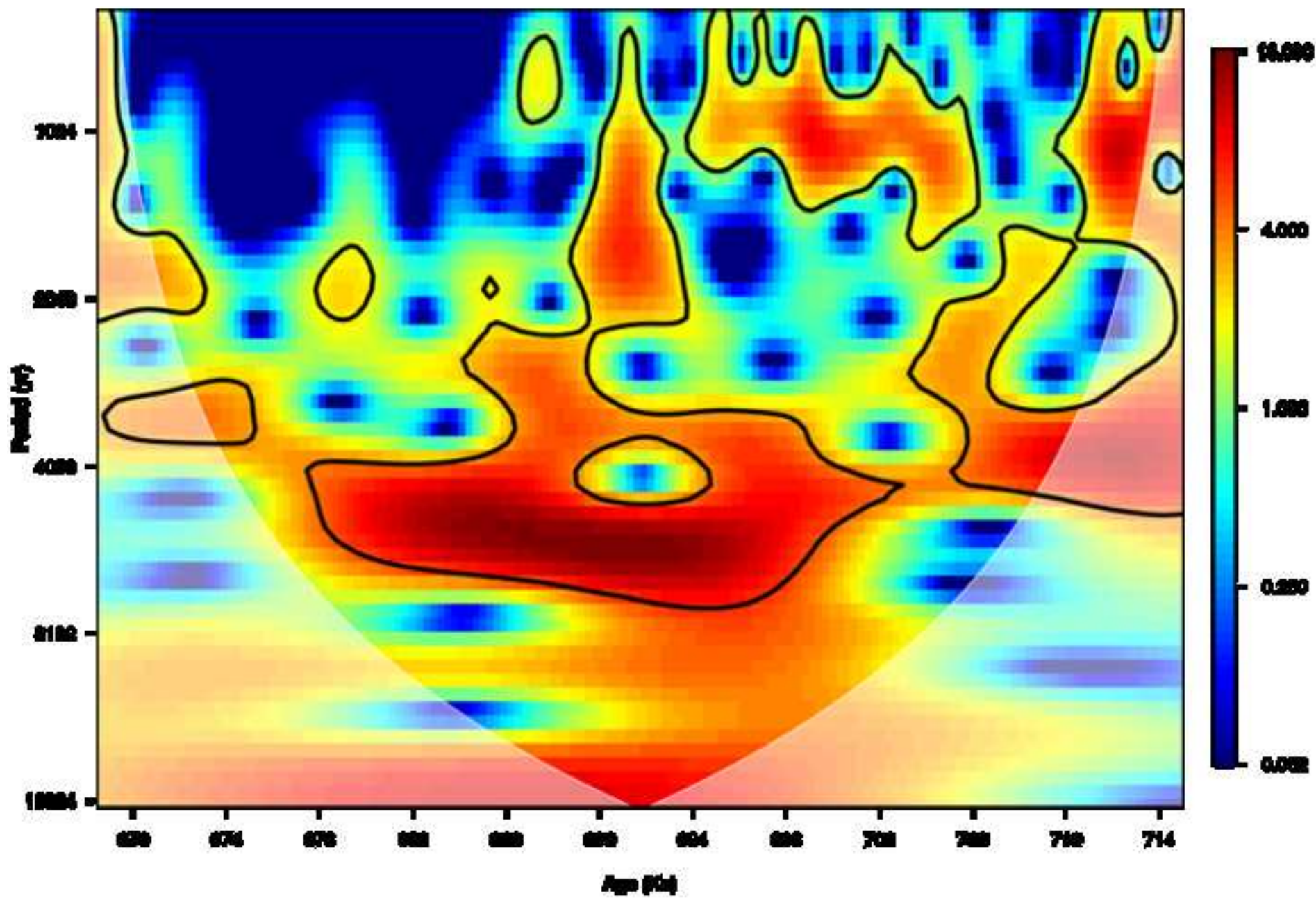


Figure 5
[Click here to download high resolution image](#)

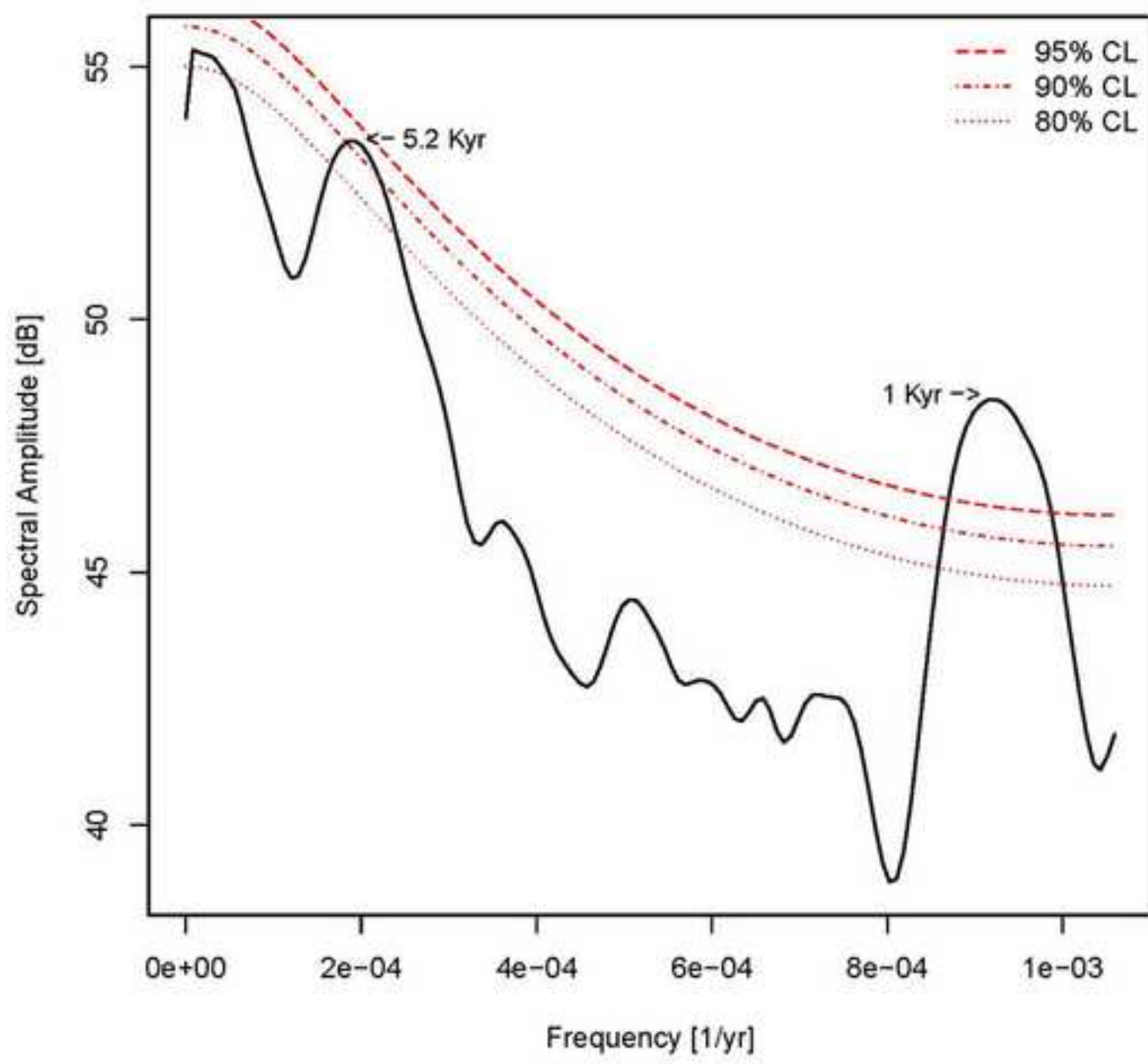


Figure 6
[Click here to download high resolution image](#)

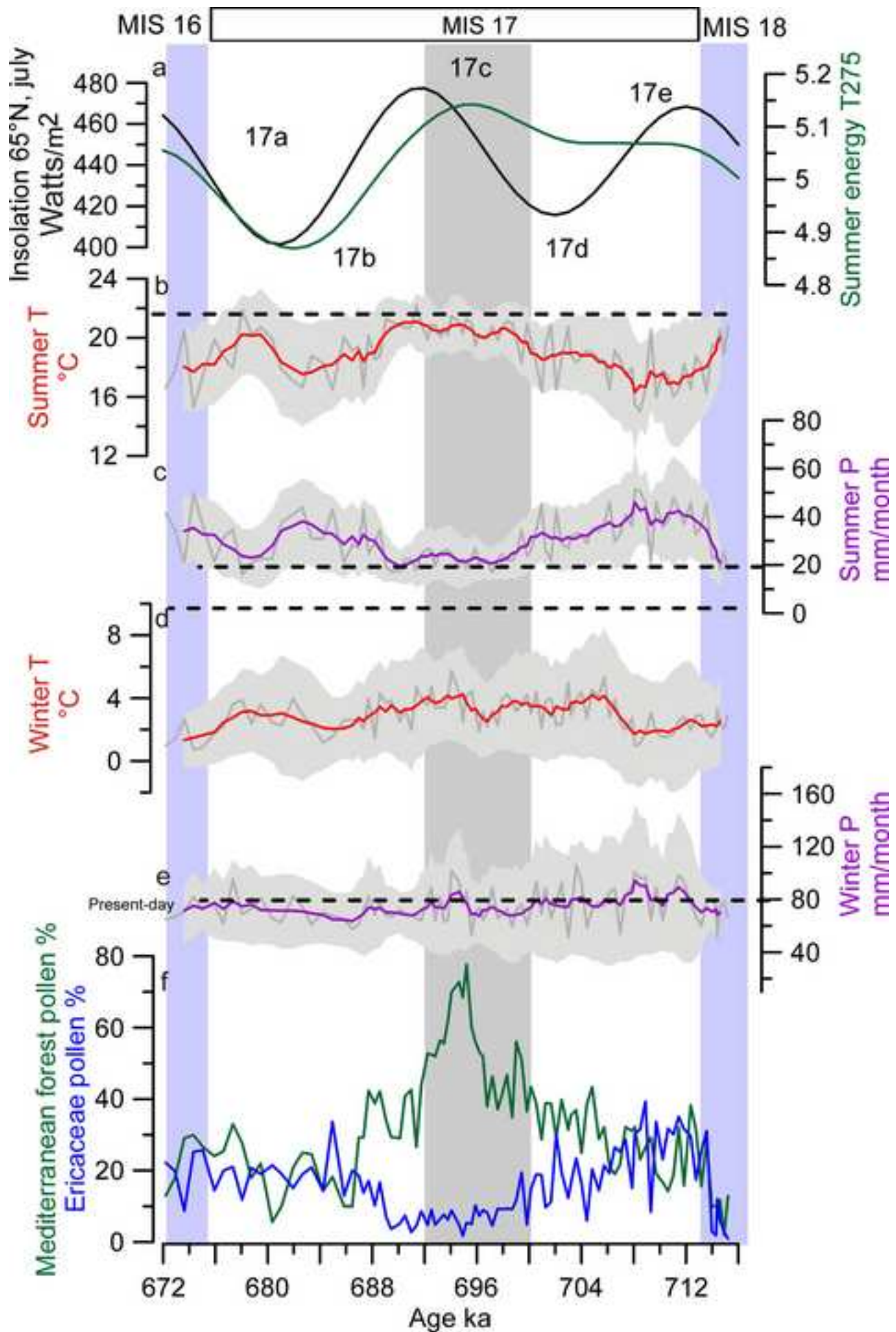


Figure 7
[Click here to download high resolution image](#)

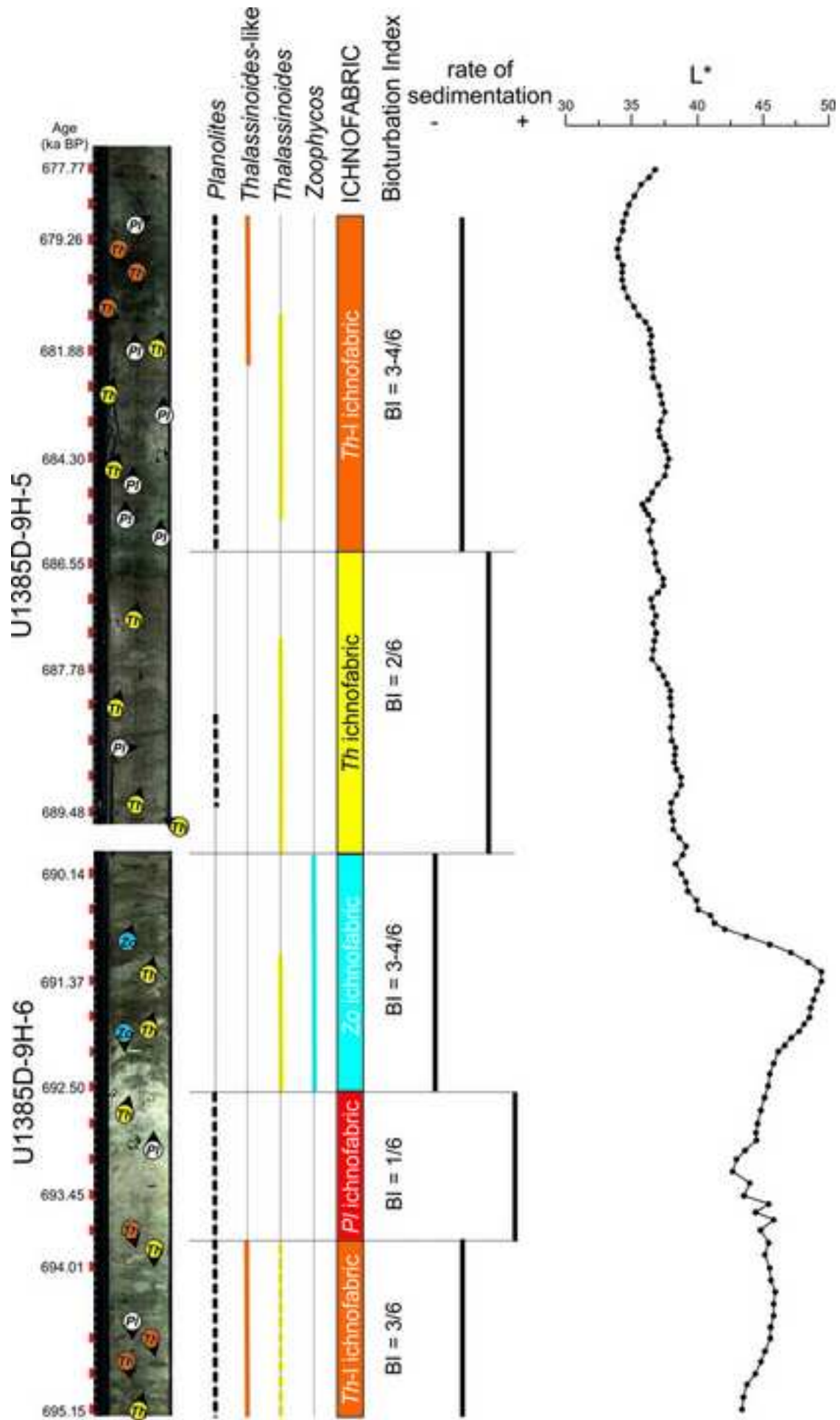


Figure 8

[Click here to download high resolution image](#)

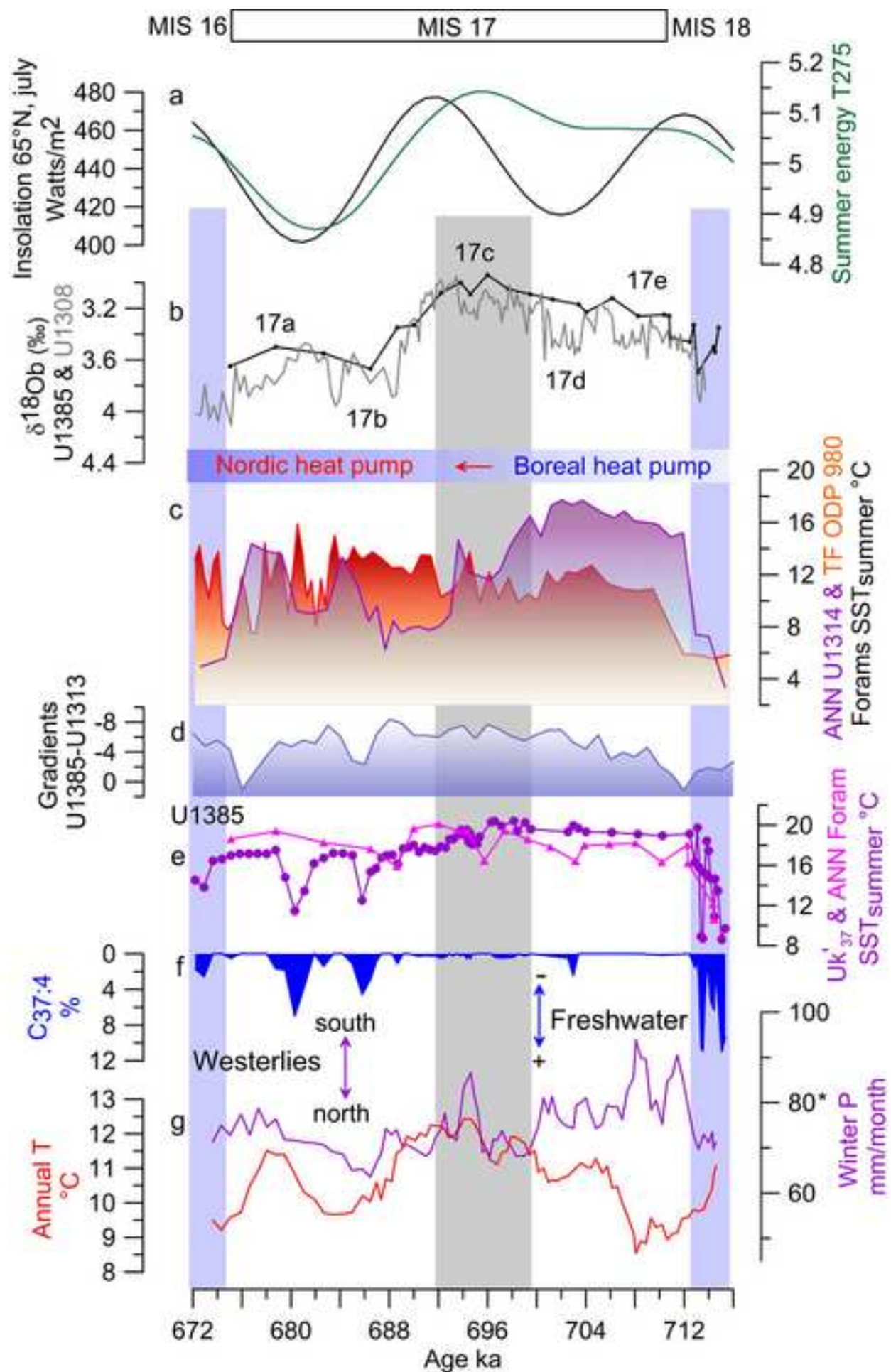


Figure 9
[Click here to download high resolution image](#)

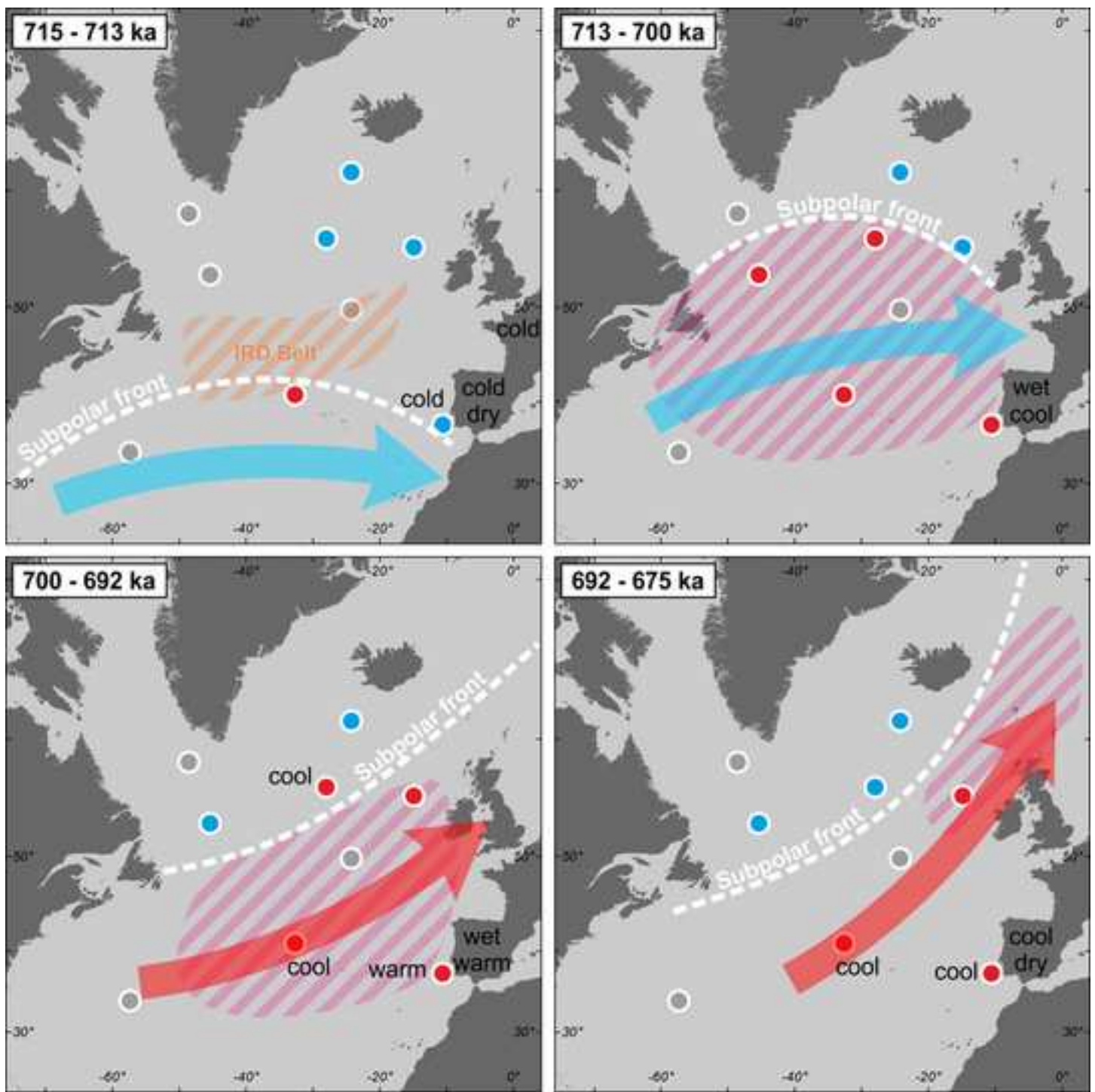


Figure (high-resolution)

[Click here to download Figure \(high-resolution\): Figure \(high resolution\) 1_Map.png](#)

Figure (high-resolution) 2

[Click here to download Figure \(high-resolution\): Figure \(high resolution\) 2_U1385_MIS 17_Alternative B_selected_rev.jpg](#)

Figure (high-resolution) 3

[Click here to download Figure \(high-resolution\): Figure \(high resolution\) 3 _U1385_MIS 17_pollen_Isot_AltB_revPoint.jpg](#)

Figure (high-resolution) 4

[Click here to download Figure \(high-resolution\): Figure \(high resolution\) 4_plot_WSP_MIS17_18dec2018_300yrs.png](#)

Figure (high-resolution) 5

[Click here to download Figure \(high-resolution\): Figure \(high resolution\) 5_MIS17_pollen_21mar2017_REDFIT.jpg](#)

Figure (high-resolution) 6

[Click here to download Figure \(high-resolution\): Figure \(high resolution\) 6_U1385_MIS 17_MATPoint_rev.jpg](#)

Figure (high-resolution) 7

[Click here to download Figure \(high-resolution\): Figure \(high resolution\) 7_New Figure \(ichnology\)_rev.jpg](#)

Figure (high-resolution) 8

[Click here to download Figure \(high-resolution\): Figure \(high resolution\) 8_U1385_MIS 17_Summer energy_MAT_SST_AltB_revF](#)

Figure (high-resolution) 9

[Click here to download Figure \(high-resolution\): Figure \(high resolution\) 9_Mars2018V3.png](#)

Table[Click here to download Table: Table 1_Age model.docx](#)

| Depth (crmcd) | Age ka (LR04) | Sedimentation rate (cm/kyr) | Hole |
|---------------|---------------|-----------------------------|------|
| 79.43 | 662.31 | 7.05 | D |
| 80.79 | 686.37 | 5.65 | D |
| 81.83 | 696.67 | 10.09 | D |
| 84.10 | 719.49 | 9.93 | A |

Supplementary material for online publication only

[Click here to download Supplementary material for online publication only: Sanchez Goni_etal_SI_EPSL_revised.docx](#)